Hydrogen Production from Rich Combustion

Haakon Pedersen-Mjaanes

Trinity Hall

Supervisor: Dr. Epaminondas Mastorakos

A dissertation submitted to the University of Cambridge for the Degree of Master of Philosophy

Department of Engineering

August 2003

Declaration

The work described herein was undertaken at the University of Cambridge's Engineering Department within the Hopkinson Laboratory between October 2002 and August 2003. This thesis is my own original work except where specifically indicated.

This dissertation does not exceed the regulation length of 15 000 words.

Dedicated to ....

I would like to express my thanks to my supervisor, Dr. Epaminondas Mastorakos, for his time, patience and invaluable support throughout this project. I would also like thank my advisor, Dr. Simone Hochgreb, for her valuable advice during reviews. I would like to thank George Biskos for his help setting up and running the SMPS. I would also like to acknowledge Rama Balachandran and Duncan Simpson for dispensing their valuable knowledge of Latex so freely.

I also appreciate the help provided by the gentlemen in the workshop for fabricating the apparatus: Michael, Trevor, John, Roy and Robert. I am grateful to my parents for their continued support. Finally I would like express my appreciation to the Chevening scholarship foundation, Bombardier and the Cambridge Engineering Department for their generous financial support.

Abstract

This paper examines rich combustion of methanol, octane and automotive-grade petrol inside inert porous media to maximize hydrogen production. Measurements of species concentrations and flame stabilization limits were tested inside several porous burners. Cordierite foam, alumina foam and alumina beads were all tested as the porous material comprising the burner.

Cordierite's melting temperature was too low to sustain the combustion temperatures inside the burner. Alumina's melting point was adequate, but alumina foam still degraded due to thermal shock and stresses being built up by the thermal cycles. The alumina beads proved much more robust as they were not rigidly constrained so did not experience the same stress build up.

The maximum conversion efficiency of methanol to hydrogen was 79% with the alumina beads and 74% with the alumina foam. The upper flammability limit of methanol was increased from 4.1 to 6.5 inside the bead burner and to 4.4 inside the foam burner. A conversion efficiency of 39% was attained for octane and petrol inside the foam burner. At a minimum, the conventional upper flammability limits of these fuels was attained. It was not possible to induce the octane or petrol flame into the beads with the current set up. A wide operating envelope with flame speeds considerably higher than for laminar free flames was observed. This allowed for a very large turndown ratio of 20:1 at an equivalence ratio of 2.5. These high conversion efficiencies without a catalyst, quick startup times and compact size make the present burner ideal for consideration as part of a reformer in a fuel cell powered automobile.

Contents

List of Figures

List of Tables

Nomenclature

Symbols and constants which are defined and used locally are not included here.

A	Cross sectional area (m^2)
ATR	Autothermal Reforming
CEA	Chemical Equilibrium with Applications
D	Diameter (m)
d_m	Characteristic cavity size (cm)
F	Shape factor
h	Heat transfer coefficient ($W/m^2 \cdot K$)
$I.C.$	Internal combustion
k	Thermal conductivity ($W/m \cdot K$)
L	Length (m)
LHV	Lower heating value
MW	Molecular weight ($kg/kmol$)
$\overline{MW}$	Average molecular weight ($kg/kmol$)
Nu	Nusselt number
P	Pressure (kPa)
Pe	*Péclet* number
PEM	Proton exchange membrane
POX	Partial oxidation
PPI	Pores per inch
ppm	Parts per million
Pr	Prandtl number

q	Heat-transfer rate (W)
Re	Reynolds number
R	Radius (m)
S_L	Laminar flame speed (cm/s)
$SLPM$	Standard litres per minute
T	Temperature (K)
UFL	Upper flammability limit
V	Velocity (m/s)
W	Watt
X	Mole fraction ($kmol/kmol$)
Y	Mass fraction (kg/kg)

Greek Symbols

α	Thermal diffusivity of gas mixture (m^2/s)
Δ	Difference
ϵ	Emmisivity
η	Efficiency (%)
ν	Kinematic viscosity (m^2/s)
ρ	Density (kg/m^3)
σ	Stefan-Boltzmann constant (w/m^2k^4)
ϕ	Equivalence ratio
ψ	Porosity (%)

Subscripts

$conv$	Convection
$corr$	Corrected
$critical$	Critical
i	Species
in	Inner
o	Outer
rad	Radiative
STD	Standard conditions
u	Unburned gas
∞	Ambient

Chapter 1

Introduction

1.1 Background and Motivation

Is a hydrogen economy viable? Even as far back as 1875, the famous French writer, Jules Vernes, in his book "L'Ile Mystrieuse" predicted that water would replace coal as an energy source, with water being split into hydrogen and oxygen to supply an inexhaustible source of heat and light (Vernes, 1875). Today numerous policy makers, energy analysts, industry leaders, entrepreneurs, and environmental organisations assert that hydrogen is the fuel of the future. In his State of the Union address on January 28, 2003, President George Bush committed 1.2 billion US dollars to help develop hydrogen fuel cell cars.

Burning hydrogen creates less air pollution than gasoline and diesel and when converted electrochemically to electricity in a fuel cell the only by-products are heat and water. Since fuel cells convert hydrogen directly into electricity they are not limited by the Carnot efficiency as internal combustion (I.C.) engines are. The most promising fuel cell to replace the I.C. engine is the proton exchange membrane (PEM) fuel cell due to its low operating

temperature, fast start up times, dynamic response and high power densities. However, the technology is still not advanced or economical enough to be commercial - particularly in the areas of production and storage.

Hydrogen is the most abundant element in the universe but little exists as a free gas on Earth. Many people in the 19th century burned a fuel called "town gas", currently known as syngas, which is a mixture of hydrogen and carbon monoxide. Several countries, including Germany and Brazil, still distribute this fuel. Globally, hydrogen manufacturing represents 2% of total world energy consumption (IEA, 2003). Currently most hydrogen is produced from fossil fuels for industrial purposes in petroleum refining, the fertiliser and other chemical industries as well fuel for the space shuttle's rocket engines. In the petroleum refinery industry, as environmental regulations have tightened and the demand for cleaner distillates has increased, heavier streams are being hydrotreated which increases the demand for hydrogen (Meyers, 1997).

Several cities in North America, Europe and Japan run hydrogen powered buses; prototype automobiles are also being tested in limited numbers. Iceland is ambitiously pursuing a goal of becoming the first country to replace their fossil fuel economy with a hydrogen economy. However, Iceland has vast thermal resources that can be harnessed to electrolyse water into hydrogen.

There are several reasons why most other countries cannot immediately switch to a hydrogen economy. Most currently do not have sufficient renewable resources to produce enough hydrogen for their economy via electrolysis. Additionally, gaseous hydrogen only contains about one fifth the energy of gasoline when stored at reasonable pressures. Finally, making the transition to a hydrogen economy means converting the existing fossil fuel infrastruc-

ture that is already developed. Problems exist using natural gas pipelines to transport hydrogen due to hydrogen embrittlement of the pipes and the very small size of the hydrogen molecule that leads to significant leakage.

One way to overcome these difficulties is through a fuel reformer. In theory a reformer can extract hydrogen cleanly and efficiently from any hydrocarbon fuel or alcohol. This would mean that cars, for example, could be powered by any number of fuels currently available, including methanol, ethanol, gasoline and even diesel; they would operate more efficiently and produce fewer emissions, at the same time creating a bridge between the future hydrogen economy and the present fossil fuel economy.

Hydrogen packs more energy per unit mass than any other fuel and produces minimum emissions when combusted and essentially no emissions when electrochemically converted to electricity in a fuel cell. It has the potential to reduce governments' dependence on foreign fuels depending on how it is generated. These are a few of the reasons why hydrogen is touted as being the fuel of the future. However, in order for hydrogen to displace fossil fuels it must be economical to produce, easy to store and get to market. Rich combustion (partial oxidation) can offer a possible technological breakthrough, through simple economical production techniques that can convert numerous fuels and alcohols into hydrogen.

One of the novel methods that can help in achieving hydrogen production from partial oxidation is combustion in porous media, this technique will be exploited in this thesis. Currently only methane has been used in porous media combustion to produce hydrogen (Drayton et al., 1998) and (Itaya et al., 2002). This research has gone a long way in proving the validity of porous media combustion and improving the understanding of the process. However, while overcoming some of the economical problems associ-

ated with transitioning to a world powered by hydrogen, it does not address the fundamental problem of having to create a whole new hydrogen infrastructure. This paper presents a method to economically produce a hydrogen rich stream from existing *liquid* fuels that can hence make use of the existing hydrocarbon infrastructure.

1.2 Methods for producing hydrogen

Since hydrogen must first be extracted from other sources, it is considered an energy carrier and not a primary energy source. Hydrogen can be separated from fossil fuels, alcohols, biomass and water using various techniques, described in detail below. This review aims to put in context the technique used in this thesis.

1.2.1 Steam Reforming

Steam reforming of natural gas is currently the cheapest method to produce hydrogen, and accounts for half of the world's production of hydrogen (Rifkin, 2002). Steam reforming is a highly endothermic reaction, used to convert light hydrocarbons with water vapour to hydrogen either with or without the presence of a catalyst according to Eq.(1.1):

$$C_nH_mO_p + (2n - p)\,H_2O \leftrightarrow \left(\frac{m}{2} + 2n - p\right) H_2 + nCO_2 \qquad (1.1)$$

The second important reaction in a steam reforming process is the water gas-shift reaction Eq.(1.2), which produces additional H_2 from water and CO.

$$H_2O + CO \rightarrow H_2 + CO_2 \qquad (1.2)$$

This reaction is dependent on temperature, with lower temperature favouring higher conversions. In the gas-shift reaction the H_2 yield is increased and the CO is reduced to $1-2\%$ (Springmann, 2002). For use in a proton exchange membrane fuel cell the CO must be further reduced to about 50 ppm in a gas cleaning process to prevent poisoning the platinum catalyst (Dupont, 2002).

1.2.2 Pyrolysis

Pyrolysis is the thermal decomposition of organic material in the absence of oxygen. It is generally seen as the first step in steam gasification of biomass (Marquevich et al., 1999) (Piskorz et al., 1988). However, research is also being conducted into a single stage process that has the potential to eliminate CO_2 emissions that the above methods suffer from. Muradov (1998) reports that catalytic pyrolysis of light liquid hydrocarbons over activated carbon yields 40-50% H_2 gas by volume.

1.2.3 Electrolysis and Thermal Water Splitting

Electrolysis is the splitting of a water molecule with electricity to produce hydrogen and oxygen. The charge breaks the bond between the hydrogen and oxygen creating ions that form on two poles: the positively charged anode attracts the oxygen, and the negatively charged cathode attracts the hydrogen. The main disadvantage of this process is that since the hydrogen is generated indirectly via electricity, efficiencies are relatively low. As a result this process is only currently economically feasible in countries that have excess hydro-generating capacity or large thermal resources. As renewable energy resources such as solar and wind become more economical they will increasingly be harnessed to produce clean hydrogen. The chemical equation

for electrolysis is:

$$2H_2O + electricity \rightarrow O_2 + 2H_2 \tag{1.3}$$

Steam electrolysis is a variation of conventional electrolysis that uses steam to provide some of the energy to split the water and increase the process's overall efficiency. Another approach to generating hydrogen is through solar-thermal which eliminates the need for an electrolyser. To disassociate water molecules using thermal energy, temperatures above 2500 K are required. Alternatively, using various catalysts this temperature can be reduced to less than 1000 K (Steinfeld, 2002). However, these last two processes are still in their infancy and currently do not produce appreciable amounts of hydrogen.

1.2.4 Thermochemical Water Splitting

Thermochemical water splitting uses chemicals such as bromine and iodine in the presence of heat to split water. Millennium Cell and Daimler-Chrysler have teamed up and powered a minivan powered by a PEM fuel cell. Hydrogen gas separated from sodium borohydride and water in the presence of heat was used to fuel the vehicle (Cropper, 2001).

1.2.5 Photoelectrochemical Processes

Photoelectrochemical processes use two types of electrochemical systems to produce hydrogen. In the first process, sunlight incident on a semiconductor electrode splits the water directly without the need for an external electrolyser (Bansal et al., 1999). In the second process soluble metal complexes are employed as catalysts. When the soluble metal dissolves, it absorbs solar energy and produces an electrical charge that splits the water. This technology

is still in the development phase (DOE, 1995).

1.2.6 Biological and Photobiological Processes

Biological and photobiological processes can use algae and bacteria to produce hydrogen. Under certain conditions, pigments in specific types of algae can absorb solar energy. The enzyme in the cell acts as a catalyst to split the water molecules thereby producing hydrogen. Photosynthetic bacteria such as Rhodocyclus gelatinosus and Rhodospirillum rubrum can perform a water-gas shift reaction to produce H_2 and CO_2 in nearly stoichiometric quantities (Maness and Weaver, 1999). This technology also holds great promise, but it must overcome the problem of the sensitivity the enzyme systems have to the oxygen produced along with the hydrogen.

1.2.7 Partial Oxidation (POX)

The combustion of a rich mixture of hydrocarbons or alcohols with a limited supply of air, either catalytically or without, is an exothermic reaction. Compared to steam reforming, much simpler and more compact reactors are possible because indirect (through a wall) heat transfer is not required. For automobile applications, the dynamic response characteristics of the POX are better than those for steam reforming. The main disadvantage of partial oxidation is the dilution of the hydrogen stream by the inert nitrogen in the air. The fuel is ideally partially oxidized to give CO, CO_2, H_2, and H_2O according to the following reactions:

$$C_nH_mO_p + \left(n - \frac{p}{2}\right)(O_2 + 3.76N_2) \rightarrow \left(\frac{m}{2}\right)H_2 + nCO_2 + 3.76(n - \frac{p}{2})N_2 \tag{1.4}$$

$$C_nH_mO_p + \left(\frac{n}{2} - \frac{p}{2}\right)(O_2 + 3.76N_2) \rightarrow \left(\frac{m}{2}\right)H_2 + nCO + 3.76\left(\frac{n}{2} - p\right)N_2 \quad (1.5)$$

$$C_nH_mO_p + \left(\frac{m}{4} + n - \frac{p}{2}\right)(O_2 + 3.76N_2) \rightarrow \left(\frac{m}{2}\right)H_2O + nCO_2 + \left(\frac{m}{4} + n - \frac{p}{2}\right)N_2 \quad (1.6)$$

In catalytic systems, the degree of conversion based on either of these reactions can be selected. In non-catalytic systems, a mixture of CO, CO_2, H_2 and H_2O is produced.

1.2.8 Autothermal

Autothermal-reforming (ATR) is partial oxidation (exothermic) followed by steam-reforming (endothermic) that equilibrates the heat of both reactions allowing the process to be driven in an autothermal mode. ATR produces a more concentrated hydrogen gas stream than POX but less than pure steam reforming. Heat transfer between the two processes allows for an overall lower operating temperature than for a straight POX and a more compact reformer compared to a straight steam reformer. ATR offers the most flexibility in heat management and potentially higher efficiencies than either of the other systems as well as a better transient response than steam reforming (Berlowitz and Darnell, 2000).

1.2.9 Gas Cleaning System

Carbon monoxide can be removed from the final gas stream by several different processes. Co-oxidation is a process where low levels of CO are oxidized

in the presence of high concentrations of hydrogen over a noble catalyst according to Eq.(1.7) (Wagner and Takeda, 2001).

$$CO + 0.5O_2 \rightarrow CO_2 \tag{1.7}$$

Depending on the selectivity of the catalyst some H_2 will also be oxidized

$$H_2 + 0.5O_2 \rightarrow H_2O \tag{1.8}$$

The following processes are discussed in more detail in (Meyers, 1997). Methanation is a reaction that converts any residual carbon oxides back to methane using a small part of the H_2 product. It takes place at lower temperatures, $200°C$, through a catalyst according to:

$$CO + 3H_2 \rightarrow CH_4 + H_2O \tag{1.9}$$

At higher temperatures a strong exothermic reaction is also possible.

$$CO_2 + 4H_2 \rightarrow CH_4 + 2H_2O \tag{1.10}$$

Gas can also be separated through membranes to a very high purity but currently only low flow rates are possible. Finally pressure-swing adsorption (PSA) can purify the hydrogen rich stream by selectively adsorbing the other gases. This process is generally quite bulky and is only applicable to stationary plants.

1.3 Porous Media Combustion

1.3.1 Theory of Rich Combustion in Porous Media

For a reformer to be used in an automobile it needs to have the same characteristics that make a PEM fuel cell suitable for the automobile industry

including: quick start up times, dynamic response, compact size, low weight and cost. This report examines a new type of POX burner that, can also be incorporated into an autothermal reformer, that has these characteristics. It uses porous media to extend the flammability limit of fuels allowing for a richer fuel/air mixture to be converted into hydrogen resulting in less nitrogen dilution in the gas stream. Since this process does not require a catalyst a wide variety of fuels can also be converted to hydrogen.

A flame can be divided into two zones: a preheat zone, where little energy is released, and a thin reaction zone, where the majority of heat is released. In free flame laminar combustion not a lot of heat is transferred to the preheat zone due to the poor heat conductivity of the gas mixture. As a result the temperature does not start increasing significantly until just before the reaction zone see Fig.(1.1). This is significant because a free premixed flame's propagation is largely dependent on the amount of heat transferred in the upstream direction.

The chemical reactions are concentrated in the reaction zone and the remainder of the combustion chamber only participates minimally in the chemical reactions. This zone can be further divided into a thin region of very fast chemistry followed by a larger region of slower chemistry. Inside the fast region the fuel is broken down into many intermediate species. This region is driven by bimolecular reactions that provide the driving force for the flame to be self-sustaining: propagation of heat and radical species. Inside the slower reaction zone, three-body radical recombination reactions occur. At atmospheric pressure the fast reaction zone is less than a millimetre, while the slower reaction zone can extend several millimeters (Turns, 2000).

The high temperature and species gradients that exist in the thin fast reaction region transport heat to the incoming gases causing them to rapidly

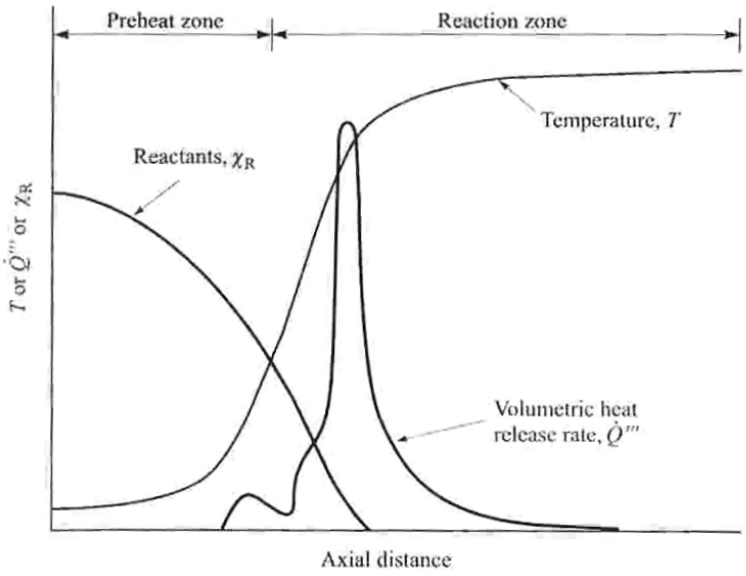

Figure 1.1: Laminar flame structure.

(Turns, 2000)

reach their ignition temperatures. In order to increase the heat transfer and make better use of the combustion chamber, turbulence can be used in the upstream gas mixture flow. However, highly turbulent flows can lead to stabilization problems, noise generation and high pressure losses.

A relatively new concept is to use a solid porous medium, which has much higher thermal and radiation heat transfer properties than the gas mixture, to preheat the reactants. Combustion in porous media transfers energy to the porous matrix upstream of the flame by conduction and radiation. This hot matrix in turn transfers energy via convection to the incoming reactants, in essence acting as an integral pre-heater.

The properties of the porous matrix depend on the properties of the material being used as porous media. Ceramic foams, ceramic beads, ceramic rings, metal foils etc. can all be used as porous media. In the combustion

region materials and porous structures with maximized heat transport properties are advantageous to extend the reaction zone. Foam structures can have porosities as high as 0.9 (Eq.1.11), while spheres have a maximum random packing density (Eq.1.12) of 0.64 or porosity of 0.36 (Weisstein, 1999). Foams have a lower optical thickness, up to 10 cavity space diameters, compared to approximately 2-3 diameters for spheres (Trimis et al., 1997). The conductivity of foams is also increased due to solid material bridges between the foams whereas for perfectly round spheres only a point contact exists between adjacent beads. Therefore, at least theoretically, foams should enhance the heat transfer properties of combustion more than beads in the combustion zone.

$$\psi = \frac{free\,volume}{total\,volume} \tag{1.11}$$

$$packing\,density = 1 - \psi \tag{1.12}$$

A single piece of foam can be used to stabilize a flame but is limited by flashback when firing at low rates. Adding a second piece of foam, upstream of the first piece, with a smaller pore size will act as a stabilizing holder for the flame and prevent flashback. The fine pores act as a flame arrestor by quenching the flame due to an increased diffusion of species and heat loss to the walls. Flame propagation is only possible when the rate of heat release from the reaction is higher than the heat loss to the surroundings. Babkin et al. (1991) found that the minimum pore size to prevent quenching inside a porous medium is only possible when the *Péclet* number exceeds a certain limit, defined by

$$Pe = \frac{S_l d_m}{\alpha} \tag{1.13}$$

By selecting a porous medium with a *Péclet* number less than the critical number for the upstream region and a Pe greater than the critical number for

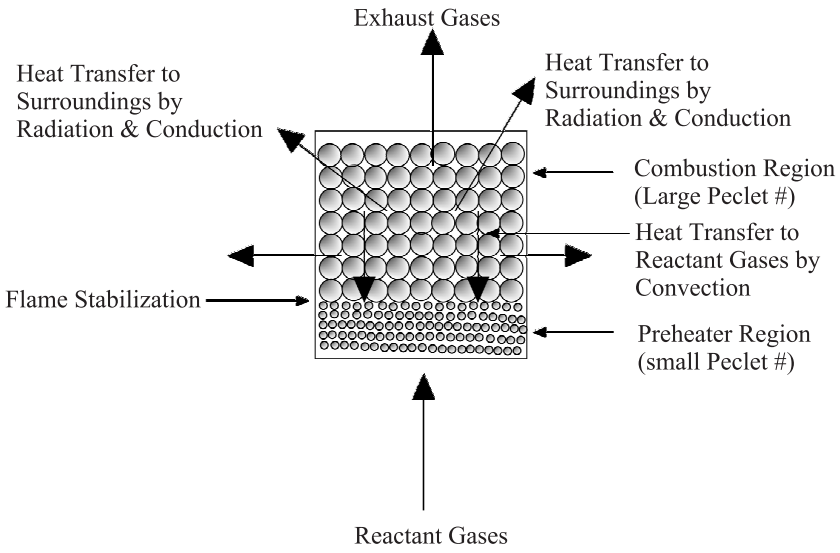

Figure 1.2: Operating principle of porous media combustion.

the combustion region, the flame will be stabilized at the interface. Fig.(1.2) illustrates this concept.

Drayton et al. (1998) and Bingue et al. (2002) observed combustion temperatures significantly higher than the adiabatic temperature predictions for a rich methane flame. They speculate that this superadiabatic combustion in the downstream propagation of the wave is caused by a redistribution of the combustion energy released by the reactants.

Diamantis et al. (2002) have developed a numerical model for planar premixed methane flames inside a porous media burner that can be used for both surface and submerged flames in the lean region. Their results predict that lean flames, ϕ=0.5, can also achieve temperatures exceeding the adiabatic flame temperature. However, at equivalence ratios close to stoichiometry flames do not experience superadiabatic combustion.

Due to the enhanced heat transport to the reactants, the flame speeds can be considerably higher than those for a laminar free flame. Zepter and Hustad

(2001), Mathis Jr. and Ellzey (2003) observed increased flame velocities for lean burning mixtures. Model results from Diamantis et al. (2002) support experimental work performed by the above investigators that higher flame speeds and hence thermal loads are possible inside porous media.

As a result of the higher velocities, elongated reaction zones are then viable because enough energy can be transported against the incoming reactants to increase the mixture's velocity. Higher flame speeds offer the possibility of more compact burners but also extension of the combustion zone which increases flame stability and hence flammability limits.

Itaya et al. (2002) were successful in increasing the upper flammability limit of methane to a ϕ of 2.5, using a single piece of alumina foam inside a burner. The reciprocal flow burner of Drayton et al. (1998) was able to support self-sustained methane-air combustion at equivalence ratios up to eight.

Trimis et al. (1997), Trimis and Durst (1996), Zepter and Hustad (2001), and Mathis Jr. and Ellzey (2003) have all investigated lean methane combustion inside a porous medium burner with two separate pieces of ceramic foam. They observed elongated reaction zones and flame stabilization at the interface between the fine and coarse pored ceramic.

The literature studied in the above paragraphs provided valuable information regarding the heat transfer mechanisms and flame propagation inside an inert porous media. In summation the principle advantages of combustion in a non catalytic porous media are:

- High heat transfer by radiation and conduction result in higher combustion velocities and cooling of the reaction zone which reduces NO_x emissions.

- Higher flame speeds, extending the combustion zone which increases

flame stability and hence flammability limits.

- Very high combustion efficiency, leading to a more compact burner.
- Homogeneous heating of the matrix which reduces hot and cold spots which are notorious for enhancing NO_x and CO_x emissions respectively.

1.3.2 Detailed Review of Combustion in Porous Media

Special attention needs to be given to the University of Illinois at Chicago's work and the Nagoya University in Japan's work as they have also looked at producing a hydrogen rich stream using porous media. The University of Illinois' reactor is a reciprocal flow burner where a mixture of air and methane is ignited and allowed to filtrate through a bed of alumina beads. The burner restricts the combustion wave to a fixed volume by periodically reversing the flow of the reactants (Drayton et al., 1998). This allows the stored energy to be used to preheat the incoming reactants. The temperature of the combustion zone then becomes a function of not only the equivalence ratio but also the filtration velocity, reactor pressure and porous bead size. The reactor used in these tests was 622mm in length and 267mm in diameter with improved results expected if a longer vessel was used.

The Nagoya University used a single piece of ceramic foam as a flame holder to help extend the UFL of a methane air mixture to produce a syngas stream. The gas mixture passes through the piece of ceramic and a flame is stabilized on its surface. The burner is a stainless steel 400mm long and 100mm in diameter vessel with a wire net placed at its exit to reduce heat losses (Itaya et al., 2002).

The technology discussed in these two papers along with the growing interest in using hydrogen as an energy carrier have provided the motivation

for this work. Tests conducted during this project use ceramic bead burners and porous foam burners to produce a syngas stream. However, in contrast to the work done by (Drayton et al., 1998) a stationary flame is stabilized inside the porous media allowing for a much more compact reformer more suited to the automobile industry. Since this work is primarily geared towards the automobile industry liquid fuels are tested instead of methane which has a lower energy density per unit mass and is more difficult to store and transport. Instead of stabilizing the flame on the surface of a low porosity piece of ceramic, a two layer high porosity ceramic burner is used where the flame is stabilized inside the ceramic between the two layers. Trimis et al. (1997), Zepter and Hustad (2001) and Mathis Jr. and Ellzey (2003) have investigated a two layer ceramic foam approach with methane for lean flames and found significant advantages concerning operational range. The fundamental idea in the two layer approach was explained in greater detail in section (1.3.1).

1.4 Objectives

The research addressed in this paper deals with converting the more difficult but much more practical liquid fuels such as methanol, octane and petrol to hydrogen. By developing a compact fuel reformer that can handle a variety of liquid fuels currently in the market place, a bridge is formed between the present hydrocarbon economy and the developing hydrogen economy. Using existing fuels allows most of the current infrastructure to remain in place while the hydrogen is generated where it will actually be consumed. For example, in the transportation industry it can be generated at the gas station or even in your car.

This technology also has applications in the petroleum refinery industry were the demand for cleaner distillates is requiring increasing hydrogen production. Additionally due to feed stock shortages of lighter fuels, hydrogen is required in hydrotreating and hydrocracking of progressively heavier feed stocks (Meyers, 1997).

The specific objectives of this paper are the following:

- To study the behaviour of flames inside several different types of porous media.
- To examine the possibility of extending the upper flammability limits of methanol, octane and petrol.
- To maximize the hydrogen production and measure the other products of combustion from these fuels.
- To test the robustness of the burner design and operational lifetime of the porous media.

1.5 Structure of the Thesis

Chapter two discusses the apparatus and method used in the experiments. Special interest is given to how the gas chromatograph (GC) functions and how it is configured and calibrated for the combustion products we are interested in. An uncertainty analysis is performed on the measurements taking during the experiments.

Experimental results and discussion are presented in chapter three. Chapter three is divided into five main sections. The first describes the flames' behaviour and the preliminary efforts to increase its velocity and upper flammability limit. The second section describes the flames' behaviour for the final

burner configuration. The third section looks at the durability and robustness of the burner and ceramics. The fourth section describes the species and concentrations obtained from the GC. These results are compared to TPEQUIL, an equilibrium model compiled by Olikara and Borman (1975). The H_2 conversion efficiency of the burners is also calculated and compared to the equilibrium H_2 conversion efficiency. In the final section, due to soot being visible in the product stream, the particulate size and mass concentration of the products from an air/octane mixture are presented.

Chapter four presents the conclusions and discusses future work to be performed on this subject.

Chapter 2

Experimental Methods

Overview

This chapter covers the apparatus used in all the experiments, the procedure followed to obtain the results and the uncertainty analysis associated with the measurements. Thermophysical properties of the fuels in their liquid and vapour states were obtained from Vargaftik (1975) unless otherwise noted.

2.1 Apparatus

The apparatus used in these experiments is illustrated in Fig.(2.1). Liquid fuel is pumped by a peristaltic pump to a commercial fuel vaporizer consisting of an injector housing and an electrically heated tube. The amount of heat delivered by the vaporizer is controlled by a variable transformer. Within the injector housing, downstream of the injector, air holes are arranged to produce a strong swirl causing the fuel to centrifuge on the bore of the tube, where it will be evaporated. Dry air is supplied by the laboratory's compressor to the injector housing. The air flow rate is measured by a rotameter

prior to entering the vaporizer. A diaphragm pressure gauge measures the pressure downstream of the rotameter so the rotameter reading can be corrected for changes in pressure (for further explanation see section 2.3.1). The vaporized fuel air mixture then enters the porous matrix burner where it is combusted. The products exiting the burner are sampled by a water cooled probe and injected into a gas chromatograph via a vacuum pump.

The entire system was leak tested and a sample of uncombusted pure methane was introduced to the gas chromatograph to ensure that it was leak tight. Had it not been leak tight an O_2 and N_2 peak would be present on the GC printout. Since the majority of tests were done at fuel rich conditions, where essentially no oxygen should be present in the products, it was easy to see on the gas chromatograph plots if a leak had developed and to rectify it.

General lab safety precautions were followed throughout the project to minimize the risks associated with combusting liquid fuels. Additionally, a local powered exhaust was used to remove any combustion products from the vicinity of the apparatus. A carbon monoxide sensor was used to periodically check for CO in the laboratory air. Polycarbonate plates were used as shielding around the burner. All gases were stored inside standard Air Product cylinders with the appropriate two stage regulators and additional shut-off valves. Only the minimum amount of fuel required to run a particular test was located near the apparatus, the rest was stored in a flammable containment cabinet in a separate room. Personal protection devices including goggles, face shield and heat resistant gloves were used when necessary.

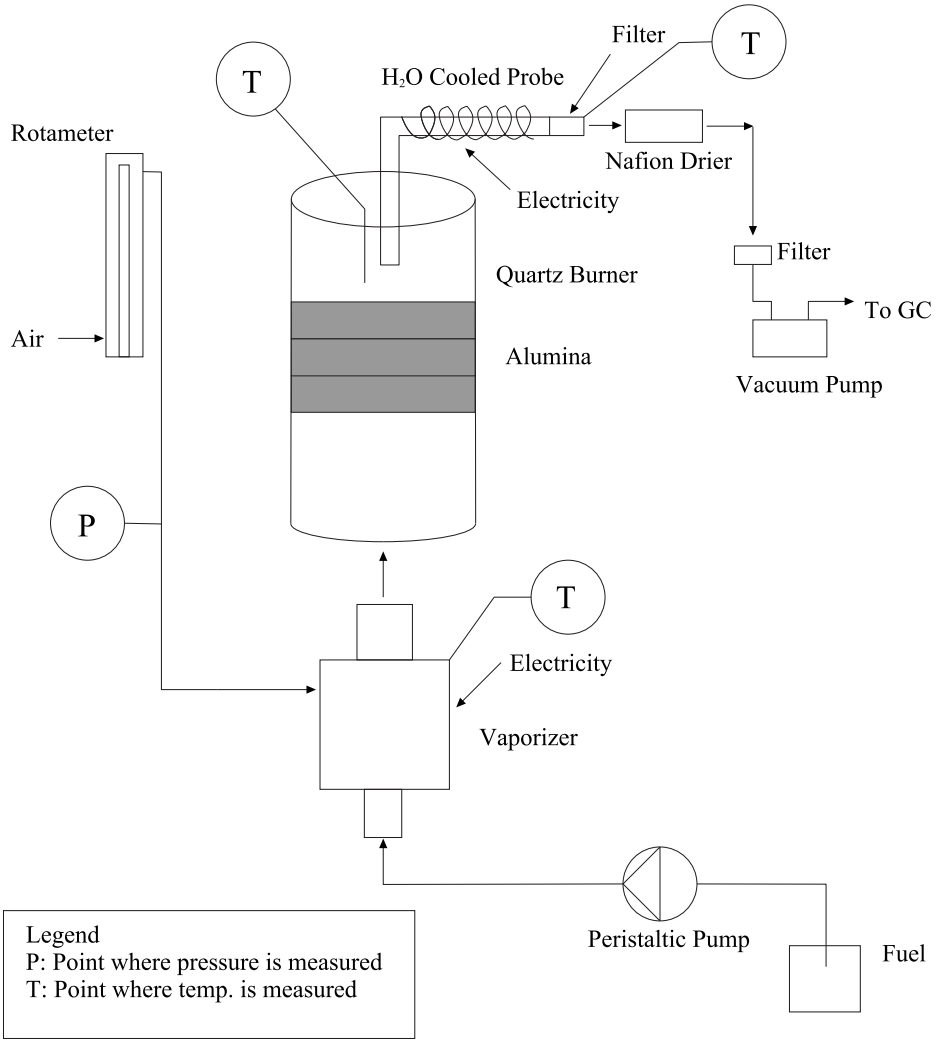

Figure 2.1: Experimental rig diagram.

2.1.1 Burner

Two types of burners were used during the course of the experiments. The first was a split stainless steel burner with an internal diameter of 29mm, illustrated in Fig.(2.2). This burner had a quartz window for viewing the location of the flame. The porous media was held inside the burner by set screws drilled through the side of the burner. The second, more successful, burner was a quartz tube with an internal diameter of 30.4mm, and an external diameter of 33.6mm, as illustrated in Fig.(2.3). In this burner the porous media was supported by a stainless steel ring attached to the top of the vaporizing nozzle. In both burners, alumina paper was wrapped around the porous foam to prevent gases leaking around the edges and to absorb some of the thermal expansion. A fine mesh was placed at the exit of the vaporizing nozzle of both burners to act as a flame trap preventing flash back.

Tests were conducted using three different types of porous media inside the burner: cordierite foam, alumina foam and alumina beads. Cordierite ceramics, $MgO-Al_2O_3-SiO_2$, are composed of approximately 13.7% MgO, 34.9% Al_2O_3 and 51.4% SiO_2. Cordierite is known for its extremely low heat expansion and high resistance to thermal shock. Fifteen percent of the earth's crust is composed of alumina, Al_2O_3, making it a very abundant and potentially inexpensive material. Alumina beads can be bought in one kilogram lots for around £20/kilogram. Alumina has a higher thermal conductivity and melting point than cordierite but also a higher thermal expansivity and lower resistance to thermal shock which needs to be considered when selecting burner material. The properties of the two materials used in this experiment are summarized in Table (2.1).

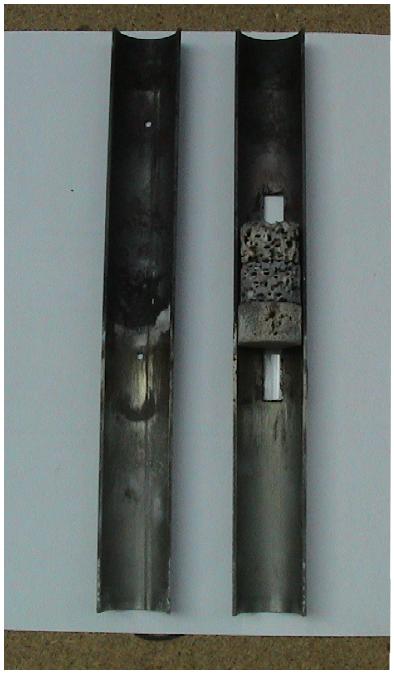

Figure 2.2: Stainless steel burner.

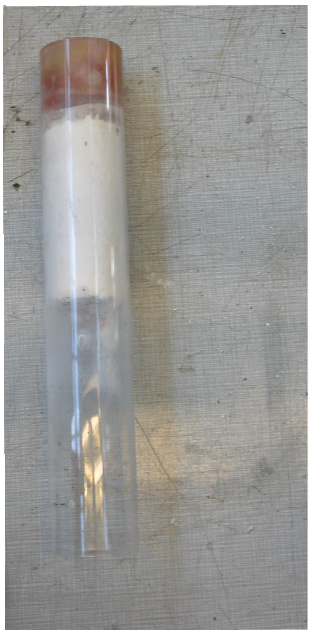

Figure 2.3: Quartz burner.

Properties	Cordierite	Alumina
Bulk density (g/cm^3)	2.1	3.9
Thermal expansivity ($10^{-6}K^{-1}$)	2-4	8.0
Thermal conductivity (W/mK)	1.2-2.5	26-35
Thermal shock resistance ($\Delta T°C$)	300	250-270
Melting temperature ($°C$)	1465	2100
Upper continuous temp ($°C$)	1300	1600-1700
Thickness (mm)	18.3	23.6
Porosity (%)	84-86	85-90
Pores per Inch (PPI)	20, 40, 60	20, 60

Table 2.1: Properties of the alumina and cordierite foams used. (Sembach, 2003; Goodfellow, 2003; Doceram, 2003)

2.1.2 Insulation

To reduce the amount of heat lost from the burner in the radial direction, insulation was applied to the burner. Heat loss through conduction decreases with R_o, but heat loss due to convection to the surroundings increases as surface area increases up to $R_{critical}$. As a result $R_{critical}$ is when heat loss is at a maximum. The critical thickness of insulation can be calculated by Eq.(2.1)

$$R_{critical} = \frac{k}{h} \tag{2.1}$$

Taking 7 W/m^2 °C (Becker, 1986) as a typical value of the convective heat transfer coefficient of natural convection in air and the conductivity for the various insulating materials as given in Table (2.2), then the critical radius of insulation for the burner is 34mm.

The heat lost per unit length of the burner can be calculated using

Material	Thermal Conductivity (W/m°K)	Thickness (mm)
Alumina paper	0.2	1.0
Quartz	1.7	1.6
Superwool607	0.24	42.0
Rockwool	0.106	50

Table 2.2: Properties of Insulation Material Used in Experiment.

Eq.(2.2).

$$\frac{q}{L} = \frac{T_{in} - T_{\infty}}{\sum_{n=1}^{n} \left[ln\frac{\frac{r_o}{r_{in}}}{2\pi K} \right]_n + \frac{1}{2\pi r_o h_{conv}}} \tag{2.2}$$

A plot of heat loss versus the outer radius is illustrated in Fig.(2.4). Due to practical limitations the final burner configuration had 95mm of insulation, detailed in Table (2.2). This plot assumes an internal wall temperature of 1200K based on measurements performed by Mathis Jr. and Ellzey (2003). For higher or lower temperatures the curve moves upwards or downwards but the trend stays the same. The heat loss for no insulation is actually considerably higher than the graph illustrates because there would be significant radiation losses especially for the quartz burner. As the insulation thickness increases the temperature of the outside layer of insulation decreases, making radiation losses trivial. The final burner and insulation configuration used is illustrated in Fig.(2.5).

2.1.3 Water Cooled Probe

The gases exiting the burner are sampled through a water cooled probe. The probe was designed to: (1) aspirate the sample from the burner with-

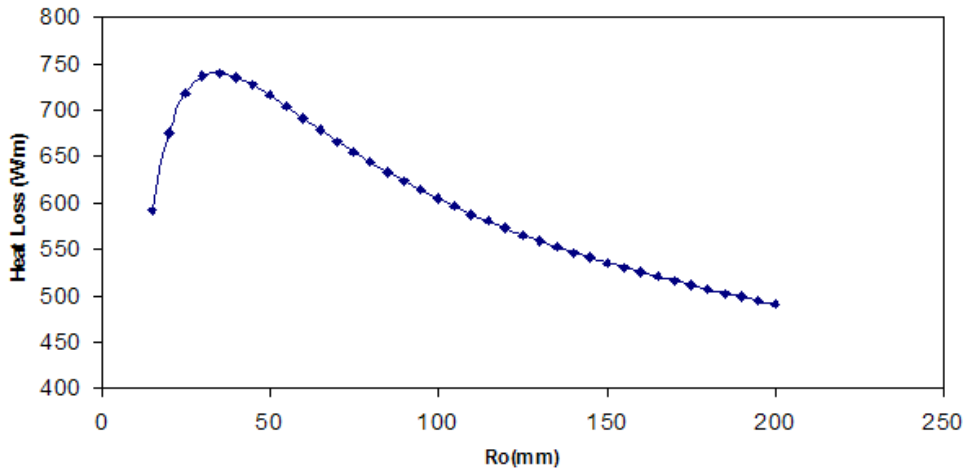

Figure 2.4: Heat loss from burner per unit length versus thickness of insulation.

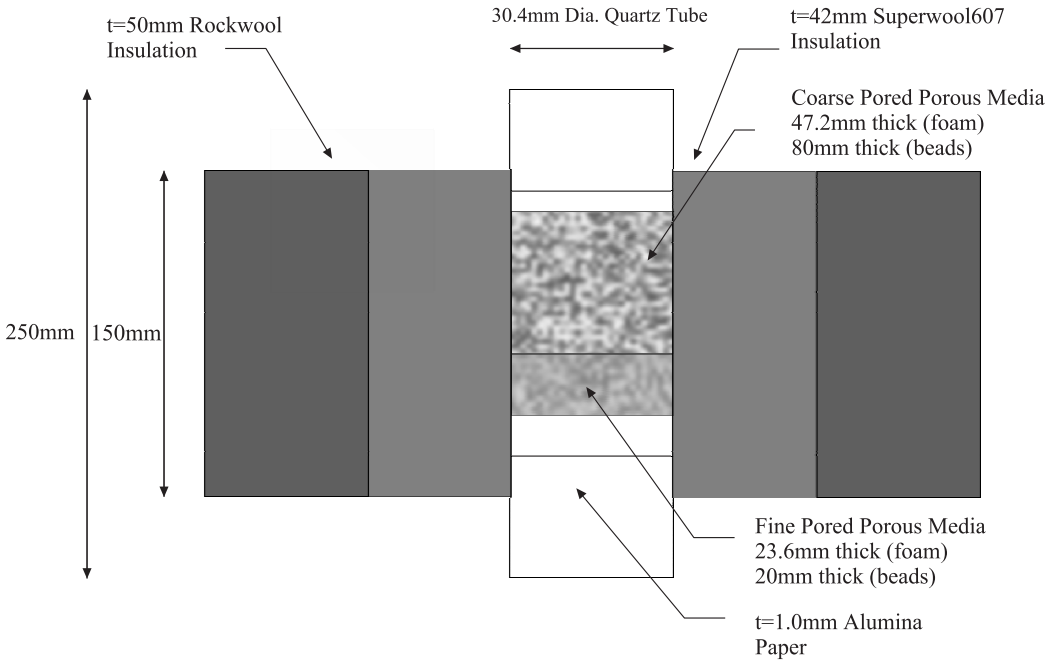

Figure 2.5: Final burner and insulation configuration used.

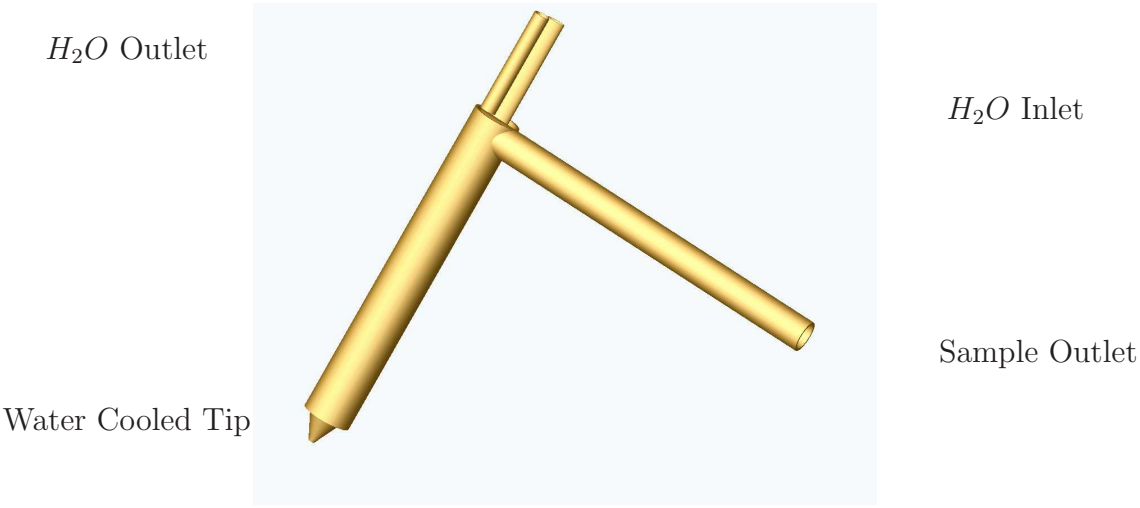

Figure 2.6: Schematic of the water cooled probe.

out disturbing the flow excessively by minimizing the probe's cross-sectional area and matching the burner exit velocity to the extraction rate, iso-kinetic sampling. (2) Deliver the sample at the probe exit without any appreciable change in chemical composition. Hence, the probe was constructed from stainless steel. (3) Freeze the reaction at the inlet of the probe by rapidly cooling it. Water from a reservoir was continually pumped into the tip of the probe via a peristaltic pump. (4) Prevent water from condensing on the inside of the probe. The downstream end of the probe was heated to maintain a temperature just above 100 °C as measured by a thermocouple at the exit of the probe. The probe is illustrated in Fig.(2.6).

Immediately after the probe a Nafion dryer was situated to remove any water from the sample prior to entering the vacuum pump and gas chromatograph. Nafion is a semi-permeable membrane that absorbs water and some polar organic substances but allows other substances to pass through unaffected making it an excellent choice for a water removal device.

2.1.4 Gas Chromatograph

Gas chromatography is a method of continuous chemical separation of one or more individual compounds between a mobile phase (carrier gas) and a stationary phase. The gas mixture enters at the injector and its different components move along at different rates. The lower the vapour pressure of the component (higher boiling point), the longer it takes to elute through the stationary phase. For these experiments an AutoSystem XL Gas Chromatograph equipped with two columns (or stationary phases) and with a Flame Ionization Detector (FID) and a Thermal Conductivity Detector (TCD) was used to measure the composition of the products. A porous polymer bead column was used to separate out the low molecular weight compounds, H_2, CH_4, CO, N_2 prior to switching the valve which transfers the gas mixture to a molecular sieve column. This column was then used to separate out the larger molecules including CO_2 and the various hydrocarbons C_2H_2, C_2H_4 and C_2H_6. The porous polymer bead column was a 1/8" inch in diameter and 5 metres long stainless steel column packed with HayeSep® N. The second column was a 1/8" inch in diameter and 1 metre long stainless steel column packed with molecular sieve 5A. The three gases used by the GC; hydrogen, zero air and the reference gas were all scientific grade gases (99.999% pure). The gas chromatograph is illustrated in Fig.(2.7).

After the components exit the column they pass through the TCD. The TCD measures the difference between the thermal transfer properties of the gas and a reference gas. In this case argon was used as the reference gas. Its thermal conductivity is high compared to hydrogen's, 0.016 W/mK versus 0.17 W/mK and also dissimilar to CO and CO_2 that were also measured with the TCD. The sample and reference filaments form two legs of a Wheatstone Bridge. A constant current is applied to the filament and as the sample

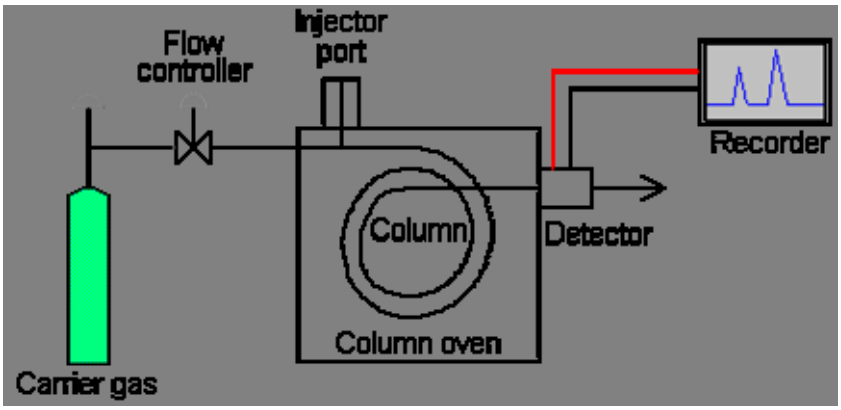

Figure 2.7: Schematic of a gas chromatograph.(Anonymous, 2002)

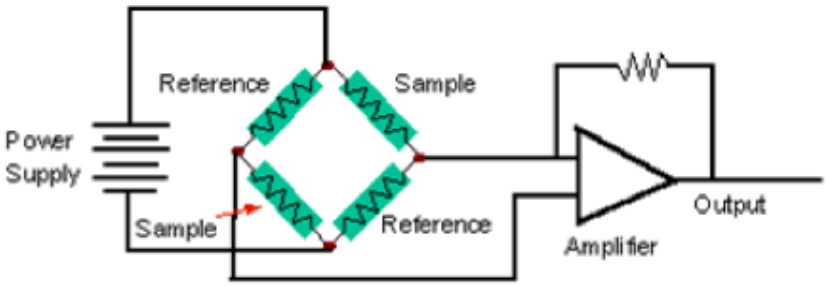

Figure 2.8: TCD diagram. (Anonymous, 2002)

passes through the detector, the resistance changes as the sample removes more or less heat than the reference gas. The response is universal since the detector responds to any compound that conducts heat. Minimum detection is 100-200ppm. The test is also non-destructive, so that after the sample passes through the TCD it can then travel on to the FID. A typical TCD is illustrated in Fig.(2.8).

A high temperature hydrogen flame ionizes compounds as they elute from the TCD into the flame. These ions are collected in the flame by applying a positive potential to the FID jet and measuring the current at the collection electrode. The response is proportional to the concentration and is measured

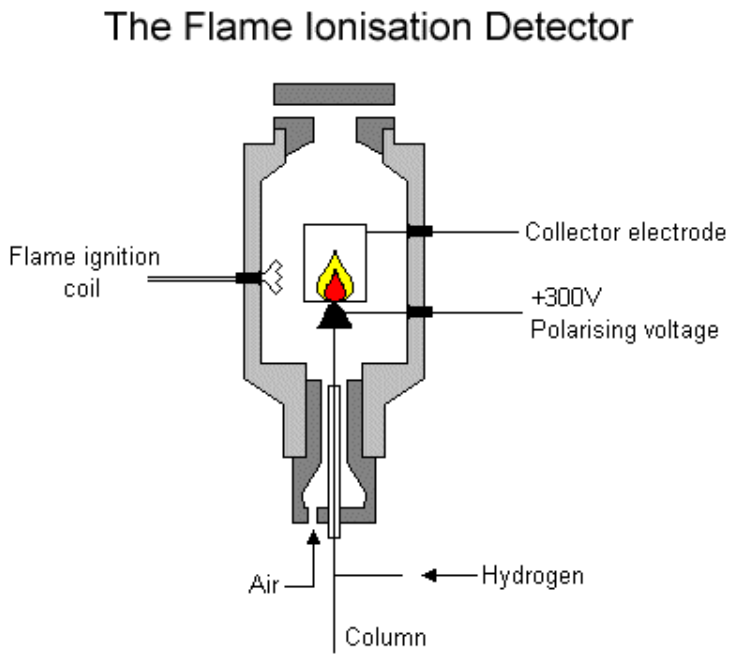

Figure 2.9: FID diagram. (Anonymous, 2002)

with an electrometer/amplifier. The FID is most sensitive to hydrocarbons and in these experiments was used to measure CH_4, C_2H_2, C_2H_4 and C_2H_6. The detector is destructive as the sample is combusted. A FID is illustrated in Fig.(2.9).

The GC was calibrated by passing two sets of calibration gases through the system. The first set contained: 1.98% C_2H_6, 2.07% CO_2, 19.92% H_2, 10.09% CO and 20.14% CH_4. The second set contained: 2.00% C_2H_2 and 1.97% C_2H_4. Ideally the GC could have been calibrated using one set of gases, however concerns of a potential reaction occurring between either the ethane and the steel container or the acetylene and the aluminum container necessitated two different sets of gases. These concentrations were chosen as this is approximately what was expected to be in the combustion products.

Fig.(C.1) and Fig.(C.2) in Appendix B are an example of a gas chro-

matograph printout of a calibration check on the GC. A mixture of 10%, by volume, uncombusted methane with air was injected into the GC. The only components detected were 10.25% methane and 0.001% ethane. The amount of methane detected was well within the uncertainty of the flow meter and the small amount of ethane could have been a trace impurity in the methane cylinder (industrial grade 99.5% purity).

2.1.5 Scanning Mobility Particle Sizer

The scanning mobility particle sizer, SMPS, consists of two stages: the classification and measurement stage. In the first stage a differential mobility analyser classifies charged particles according to their ability to transverse an electric field. Depending on their charge, positive or negative, particles are either attracted or repelled by a central column located inside the differential mobility analyser. Particles within a narrow band of electrical mobility diameter, exit through a slit at the end of the column and travel to the second stage. By varying the central column voltage, particles of different mobility are sent to the next stage, allowing a size distribution to be produced. In the second stage a condensation particle counter optically measures the concentration of the particles. The entire process takes on the order of a minute to complete (Biskos, 2001).

2.2 Procedure

At the start of each experiment the vaporizer was heated to its operating point with just air passing through it. Once the vaporizer was above the vaporization temperature of the fuel, the fuel pump was activated and the air-fuel mixture flowed into the burner. The mixture was ignited with a

butane torch at the burner's exit. A slightly richer than stoichiometric flow, highest temperature and flame speed, was used to induce the flame into the porous media. After the flame had stabilized at the interface between the support layer and the combustion layer the flow was held constant for several minutes to allow the burner to warm up.

After the warm up period, the flows were adjusted to their desired values for the experiment. After an additional period of several minutes the system reaches thermal equilibrium, which can be deduced by constant thermocouple readings and a stationary flame front. The two thermocouples used in determining this were a K-type thermocouple imbedded inside the vaporizer and an R-type thermocouple located 10mm above the ceramic. At this point a gas sample can be injected into the gas chromatograph. Following the ignition of the gas mixture, the vaporizer's temperature, temperature at the outlet of the burner, fuel and air flow rates were recorded manually at one minute intervals. The products' composition was recorded by TotalChrome, the Gas Chromatograph's software.

2.3 Experimental Uncertainty

In all experimental work errors will creep into the data. Every measurement that is taken has some uncertainty associated with it. During this project every reasonable effort was made to keep errors to a minimum by regularly calibrating equipment, repeating various experiments, not indiscriminately discarding data, only varying one variable at a time and most importantly using great care and patience throughout the course of the project. Much of the error in a measurement can be eliminated by regular calibration. However, this will only improve its accuracy up to the precision of the instrument.

The accuracy of an instrument indicates the deviation from a known input. The precision of an instrument indicates its ability to reproduce results with a given accuracy.

2.3.1 Rotameters

Two rotameters each with an accuracy of ± 2% full scale deflection were used to measure the air flow entering the vaporizer. A rotameter works on the physical principle of drag, balancing the force of gravity against the force induced by the flowing medium on the bob. The meter is calibrated for a particular fluid, in this case air, at standard pressure and temperature. As a result any deviation from these conditions must be taken into account. A corrected flow rate can be calculated using Eq.(2.3).

$$Q_{corr} = Q \left[\frac{P}{P_{STD}} \frac{T_{STD}}{T} \right]^{0.5} \tag{2.3}$$

The first meter was used for flows in the range of 2.5 to 20 slpm. The second for flows less than 2.5 slpm. Due to the pressure drop through the vaporizer and porous media a back pressure resulted at flows greater than 8 slpm. As a result these measurements must be corrected with Eq.(2.3), but have an error associated with the pressure gauge as well as the error from the flow meter itself. The pressure gauge has an accuracy class of 1.6 or is accurate to within ± 1.6%.

2.3.2 Fuel Pump

The pump used to convey the fuel is a Watson/Marlow 101U/R peristaltic pump with a digital potentiometer used to control the flow rate. This pump has an accuracy of ± 2% of the flow rate. The pump was calibrated a

minimum of three times using a stopwatch and beaker every time a new fuel was used.

2.3.3 Gas Chromatograph

The uncertainty associated with the gas chromatograph is harder to define. The uncertainty is at least ± 2% as this is the uncertainty associated with the calibration gases. The instrument's conditions are optimized by ensuring the following: (1) there are no leaks from the probe to the GC that the sample is extracted through, (2) the columns are giving good reproducible separations of the components, (3) there is no carryover of components or contamination, (4) all supplies of gas and power to run the system are stable and (5) the samples are being introduced in a standard reproducible way, i.e. all injected using the same technique, sample loop size, temperature and pressure.

After ensuring the above it is difficult to separate any uncertainty associated with the GC from uncertainty associated with the rotameters and fuel pump. Repeating a test several times under the same conditions gave product compositions within the error bands associated with the flow meters.

2.3.4 Thermocouple

In this experiment only one R-type thermocouple was used to measure the flame temperature, its location is illustrated in Fig.(2.10). Due to the nature of the experiments the distance between the flame and the thermocouple varied depending on equivalence ratio and the mass flow rate of gases. As a result the thermocouple was only used to determine the direction the flame front was moving in and to ensure that the flame was stable prior to any measurements being taken. Chapter 4 will discuss ways to improve temperature

measurement for future work.

However, it is still important to see how accurately the thermocouple can read the gas temperature at its fixed location. The thermocouple itself is very accurate ($\pm$ 1.5°C from 0 to 1100°C). A thermocouple measures the temperature of the thermocouple bead, which may vary from the actual temperature of the gas stream at high temperatures where radiation losses and gains must be balanced with conduction and convection heat transfer. The following calculations assume: (1) no evaporation (i.e. the thermocouple is dry) (2) thermocouple is isothermal (3) system is at equilibrium and (4) conduction losses along the thermocouple wire are negligible. A large thermal gradient between the thermocouple wire and bead did not exist as both were in a moving gas stream at approximately the same distance above the ceramic. The rule of thumb is that if the exposed wire is at least ten times longer than the diameter of the wire, as it is in this case, then the conduction losses will be minimal (Anonymous, 1994).

The thermocouple and its surroundings can be broken down into four main areas: (1) The burner surface (2) the thermocouple bead (3) the ambient environment and (4) the insulated walls of the burner. This is illustrated in Fig.(2.10). The energy emitted by the burner and absorbed by the thermocouple bead is calculated by Eq.(2.4)

$$Q_{12} = \sigma \varepsilon_1 A_1 F_{12} T_1^4 \alpha_2 \tag{2.4}$$

where σ is the Stefan-Boltzmann constant equal to 5.669x10-8 W/m^2K^4, ε_1 is the fraction of energy emitted by the burner, A_1 is the surface area of the burner, F_{12} is the fraction of energy emitted by the burner that strikes the thermocouple bead, T_1 is the temperature of the burner's surface and α_2 is the fraction of energy absorbed by the thermocouple bead.

All of the above variables can either be measured or looked up in reference

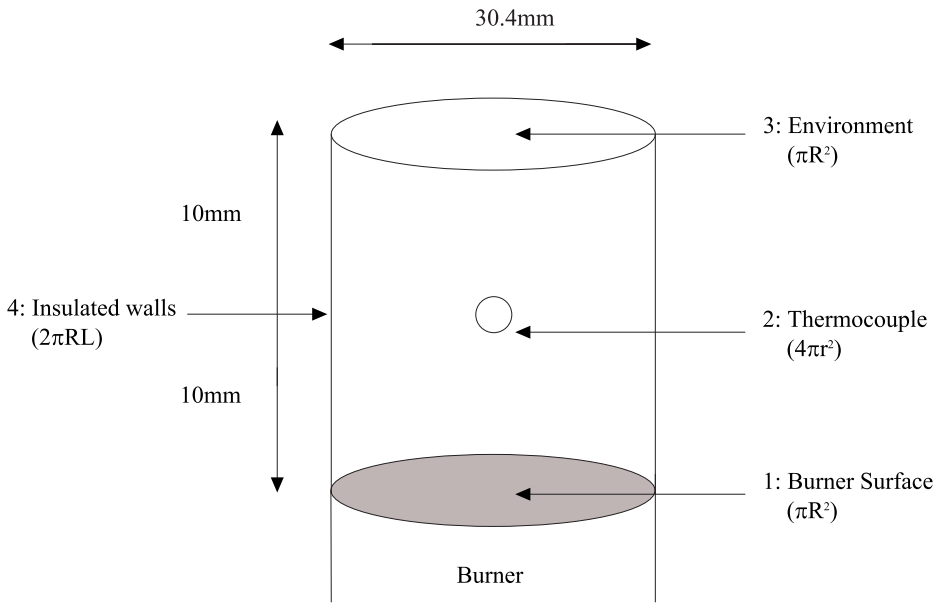

Figure 2.10: Location of thermocouple bead with respect to burner.

books except for T_1, which must be estimated, and the shape factor, F_{12}, which can be calculated. The shape factor from the thermocouple bead to the other three surfaces must be unity since the thermocouple is completely surrounded by these three shapes. The shape factors can be calculated using the following formulas:

$$F_{2\to4} = \frac{2\pi RL}{2\pi RL + 2\pi R^2} \tag{2.5}$$

Through symmetry

$$F_{2\to1} = F_{2\to3} = \frac{1 - F_{2\to4}}{2} \tag{2.6}$$

Through reciprocity

$$F_{3\to2} = F_{1\to2} = \frac{A_2}{A_1} F_{2\to4} \tag{2.7}$$

$$F_{4\to2} = \frac{A_2}{A_4} F_{2\to4} \tag{2.8}$$

The Nusselt Number, (Nu), for forced convection flow past a sphere may be calculated using Eq.(2.9) which is valid for:

$3.5 < Re < 8x10^4$

$0.7 < Pr < 380$

$$Nu = 2 + (0.4Re^{0.5} + 0.06Re^{0.67})Pr^{0.4} \tag{2.9}$$

where Re is defined as

$$ReynoldsNumber = \frac{VD}{\nu} \tag{2.10}$$

The convective heat transfer coefficient may be solved for using equation Eq.(2.11)

$$h = \frac{kNu}{D} \tag{2.11}$$

Where k is the thermal conductivity of air and D is the diameter of the thermocouple bead.

Using the above equations the net energy absorbed by the thermocouple can be calculated. Equation (2.12) can then be used to balance the energy absorbed from radiation to the energy removed by convection, hence calculating the actual temperature of the gas stream around the thermocouple.

Since conductivity along the wire is assumed to be negligible, setting the energy due to radiation equal to the energy due to convection, the temperature of the gas can be solved for.

$$Qrad = Qconv \tag{2.12}$$

Fig.(2.11) illustrates the thermocouple error depending on the surface temperature of the burner. Diamantis et al. (2002) calculate that the burner surface temperature should be less than 1500K. Based on this, the error due to radiation and convection is minimal. Therefore, temperature readings used

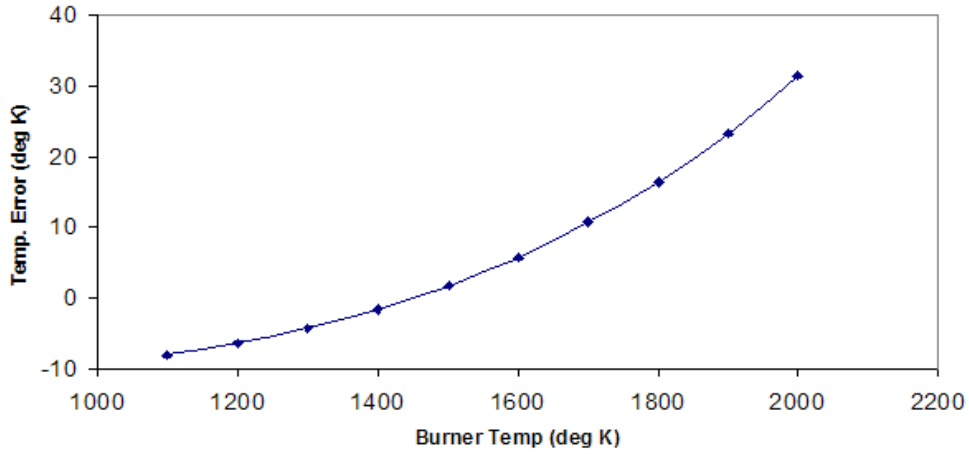

Figure 2.11: Thermocouple error due to radiation and convection.

throughout the remainder of this paper will not be corrected for radiation or convection errors.

2.3.5 Error Derivation

To assess the uncertainties contained in the data, an error analysis was performed on both the air and fuel flow rates. The corrected air flow rate, Q_{corr}, is a function of the measured flow rate, Q, and the pressure, P. Using the method described in Kline and McClintock (1953) the uncertainty in the measurements can be calculated by Eq.(2.13). The example below is specific to the uncertainty contained in the air rotameter. To calculate the uncertainty in the equivalence ratio the formula is amended to include a term for the fuel flow rate.

$$W_{Qcorr} = \left[\left(\frac{\partial Q_{corr}}{\partial Q} \omega_q \right)^2 + \left(\frac{\partial Q_{corr}}{\partial P} \omega_p \right)^2 \right]^{0.5} \tag{2.13}$$

The uncertainty of the equivalence ratio, ϕ, is a function of the error associated with the rotameter, pressure gauge and fuel pump can be calculated using Eq.(2.14).

$$W_\phi = \left[\left(\frac{\partial \phi}{\partial Q_{Qcorr}} \omega_{Qcorr} \right)^2 + \left(\frac{\partial \phi}{\partial Q_{pump}} \omega_{Qpump} \right)^2 \right]^{0.5} \tag{2.14}$$

The largest uncertainties are associated with the air rotameters, especially at low flow rates just prior to switching to the smaller rotameter. These low flow rates are associated with high equivalence ratios. A maximum uncertainty of ±15% at an air flow rate of 2.75 SLPM was calculated. This corresponds to an overall uncertainty for ϕ of ±16%. At higher flow rates, lower equivalence ratios, the uncertainty decreases so that at a half scale deflection of 10 SLPM the uncertainty associated with the rotameter has reduced to ±7%.

Chapter 3

Results and Discussion

3.1 Preliminary Testing

Section 3.1 summarizes the preliminary testing conducted prior to selecting a final burner configuration. Section 3.2 discusses how the flames behaved inside the porous media for the various fuels and ceramics tested. Section 3.3 describes how the burner and in particular the ceramics endured the testing. Section 3.4 details the product species and concentrations that the GC detected. The final section, 3.5, comments on the concentration and particulate size from combusting octane at various equivalence ratios.

3.1.1 Methanol

Methanol, CH_3OH, is the simplest of the alcohols and is viewed as a potential energy carrier for the automobile industry. It is an intrinsically pure product, has a higher flame velocity and wider flammability limits than petrol.

Cordierite

Initially, a single piece of 18.3mm thick cordierite was used inside the steel burner to carry out a set of feasibility tests. It should be noted that in these tests the UFL was considered to be the richest flame that could be stabilized. During these tests the flammability limits of methanol were not extended. This can be attributed to insufficient burner insulation, failing of the ceramic cement and only a single piece of foam resulting in a surface stabilized flame without the advantages of a submerged flame inside the porous media.

In the second set of tests a piece of 60 PPI cordierite was placed upstream of a 40 PPI cordierite and secured in place by alumina paper instead of ceramic cement. The flame stabilized on the surface of the top piece of ceramic but would not penetrate further down. In this instance the flame could not propagate into the ceramic because it was losing more heat to its surroundings than it was generating. Or put another way, the *Pé* number was too low to allow the flame to propagate into the ceramic. The top piece of foam was replaced with a 10 PPI piece of cordierite and in this case the flame stabilized at the interface between the two ceramics. Fig.(3.1) is a photo of the flame descending down towards the cordierite interface. The thermocouple and top piece of ceramic are glowing. Fig.(3.2) is a photo of the flame once it has stabilized at the interface. The two white bands around the foam pieces are alumina paper.

The quartz window of the first burner cracked after only a couple of thermal cycles due to the differing thermal expansivity of the stainless steel burner (16-18x$10^{-6}K^{-1}$) and quartz window (0.75x$10^{-6}K^{-1}$). The cracks are visible in Fig.(3.1). Another problem with the first burner was that the split tube design leaves egress routes for air to enter the burner or gas to escape. An all-steel burner constructed without a split was considered but rejected,

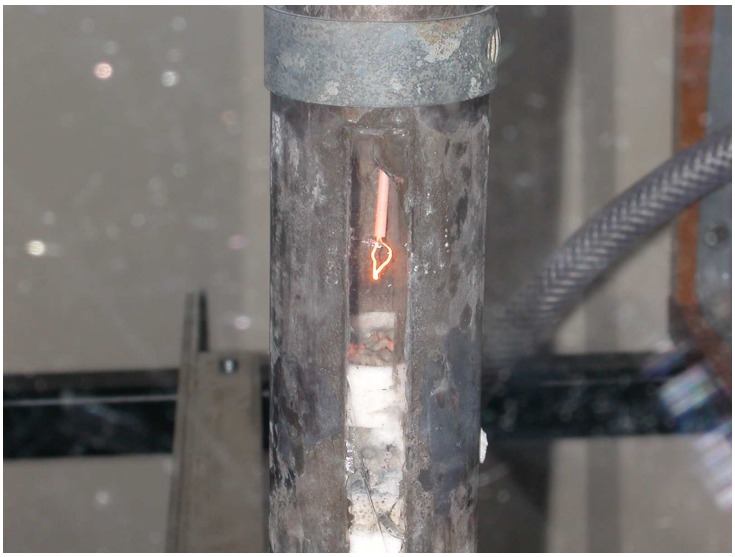

Figure 3.1: Methanol flame descending towards interface.

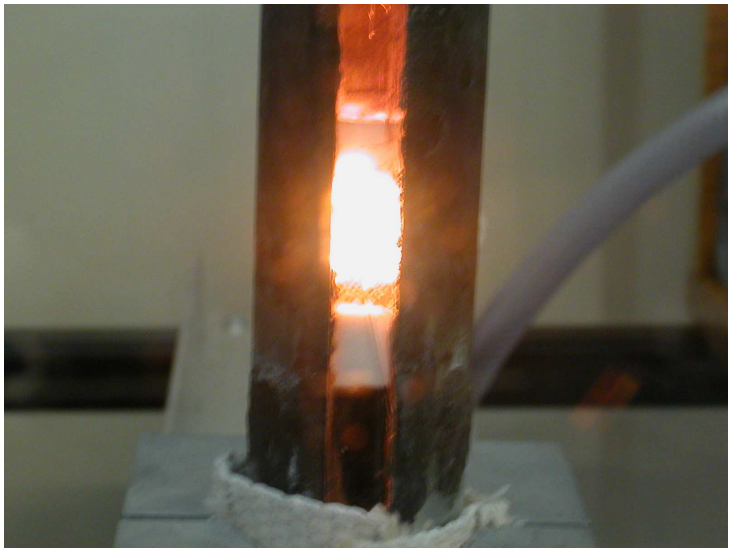

Figure 3.2: Methanol flame stabilized at ceramic's interface.

since being able to see the location and colour of the flame is important with an experimental apparatus. As a result a quartz tube burner was selected due to its transparency, high softening temperature (1800K) and excellent thermal shock characteristics (Mindrum Precision, 2003).

The ceramic was transferred into the new quartz burner and an attempt to repeat the second set of tests in the steel burner failed. The flame would not enter the 10 PPI top piece of ceramic. It was assumed that this was because the radiative heat losses were too excessive through a transparent burner. This hypothesis was proven correct when 40mm of Superwool insulation was added to the outside of the burner and the flame stabilized once again at the interface between the two ceramics. However, after several more thermal cycles the flame became increasing difficult to stabilize at the interface. Inspection of the cordierite revealed that the centre of the top piece had melted.

As can be seen from Fig.(3.3) the inside of the top piece sustained the most damage, as would be expected since this is where the reaction is occurring. The axial surface is essentially intact suggesting that a large temperature gradient exists extending from the centre out towards the walls of the vessel. This also implies that additional insulation may be required. At this point testing with cordierite terminated and testing with alumina commenced.

3.2 Flame Characteristics

Alumina Foam

Tests in the same burner using one 60 PPI piece of alumina foam as the flame holder and one 20 PPI piece of alumina downstream of it produced results similar to the latest cordierite tests. The flame would stabilize at the interface

Top piece

Bottom piece

Figure 3.3: Damaged pieces of cordierite.

but it was not possible to extend the flammability limits. A maximum UFL of 3.5 was achieved. According to the literature (Turns, 2000) the UFL for methanol is 4.08. Each piece of alumina had a thickness of 23.6mm.

At the lower flow rates the reaction was losing more heat to its surroundings than it was generating and the flame would gradually fade and then disappear. At the higher flow rates the flame front would start moving up towards the surface and blow off would occur. It should be noted that at low flow rates and conditions closer to stoichiometric conditions, the reaction could generate enough heat to penetrate the bottom piece of ceramic and flashback would occur.

A wire net was placed over the exit of the burner, to determine if the limit could be increased further as was done by Itaya et al. (2002). A slight improvement was noticed, indicating that radiative heat losses from the surface

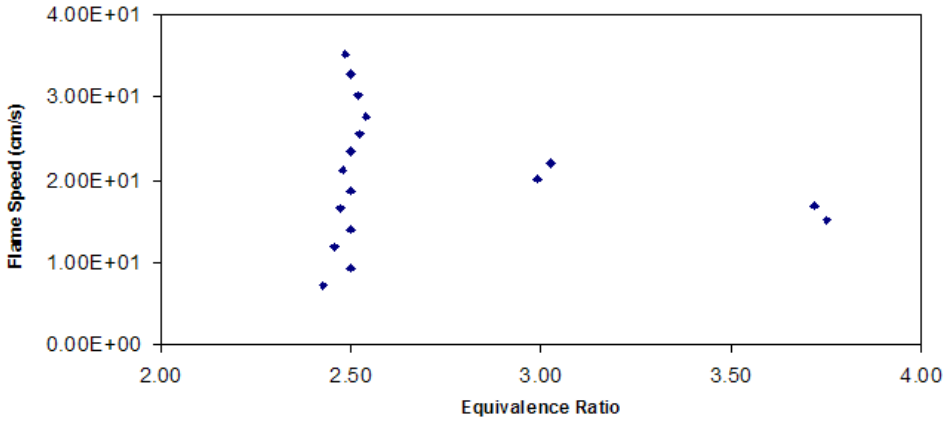

Figure 3.4: Operating envelope of methanol with three pieces of alumina foam.

of the 20 PPI piece of ceramic were still excessive.

Next a second piece of 20 PPI alumina foam was added on top of the single piece of 60 PPI foam. In this set-up the flame still stabilized at the interface between the fine and coarse ceramic. This resulted in more radiant heat being trapped inside the burner, increasing the energy available to heat the incoming gas mixture. Tests of this configuration increased the UFL to 3.8. In this instance placing a metal screen over the exit produced no improvement. Hence, this configuration of a single piece of 60 PPI alumina foam and two 20 PPI pieces of alumina foam without a metal screen at the outlet was used for the remainder of the ceramic foam tests. The operating envelope is illustrated in Fig.(3.4) for equivalence ratios equal to or greater than 2.5.

At this point, 50 mm of rockwool insulation was added to the existing insulation. This configuration was used for the remainder of the tests and is summarized in Table (2.2). With the increased insulation the UFL was

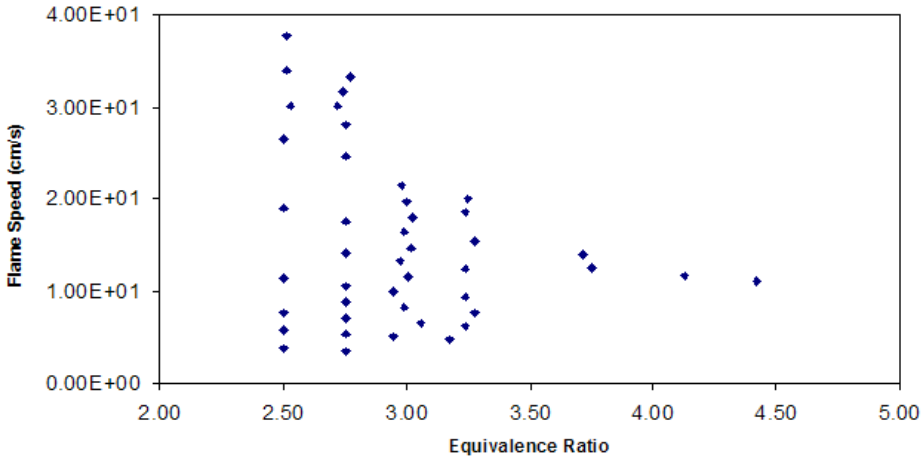

Figure 3.5: Operating envelope of methanol with two pieces of alumina foam and increased insulation.

extended to 4.4. The operating envelope became wider, as well as extending further to the right Fig.(3.5). The flame's stability increased compared to the previous test for both higher and slower flow rates due to less heat being lost to the surroundings.

In porous media combustion, an operating envelope is possible as opposed to a unique burning velocity for each ϕ as occurs in a premixed laminar free flame. Consider the various flame speeds at a ϕ of 2.5 in Fig.(3.4). The expected flame velocity will be higher than that for a free flame because of the aforementioned enhanced preheating of the reactants. If the flow of reactants are reduced the flame will attempt to move further upstream, but because of the fine pored ceramic will not be able to propagate into it. Additionally, the lower reactant mass flow rate will mean less energy is available to preheat the incoming gasses. These two mechanisms will reduce the flame's speed and allow it to stabilize at the interface as long as the amount of heat being released by the reaction balances the amount lost to the surroundings.

If the flow of reactants is increased the flame will propagate downstream away from the fine pored ceramic where less heat will be absorbed by the ceramics, therefore increasing the preheating of reactants. Also the increased mass flow rate will increase the amount of energy being released by the reactants. Both of these mechanisms will increase the flame's velocity and act as a restoring force on the flame moving it back towards the interface.

As is expected the envelope narrows with increasing ϕ. As ϕ increases, the energy released by the reaction per unit mass of mixture decreases as less O_2 is available to complete the process. This results in less energy being available to preheat the incoming gases contributing to slower flame speeds and limiting the number of stable operating points. The opposite happens as flow ratios approach stoichiometric conditions. Equivalence ratios lower than 2.5 were not tested due to safety concerns with the high heat output.

A plot of laminar flame speeds versus ϕ, Fig.(3.6), based on a derivation from (Metghalchi and Keck, 1982), can be compared to flame speeds inside the porous media: unfortunately the correlation is only valid for ϕ=0.8-1.4. Appendix A has more details on the formulas used to calculate the velocities for the above figure. Inside a porous medium the flame can be stabilized over a range of velocities. Fig.(3.5) illustrates that at a ϕ of 2.5 the range varies from less than 5cm/s to as high as 40cm/s. Based on the above calculations the richest point that we have data for is 1.4 which corresponds to a flame speed of 35cm/s. This demonstrates that flame velocities higher than the laminar free flame velocity are possible, in agreement with Zepter and Hustad (2001) and Mathis Jr. and Ellzey (2003).

Holding the ϕ constant while increasing the flow rates results in more energy being released by the reaction. Fig.(3.7) illustrates the increase in temperature with an increase in flame speed. Additionally, the flame front

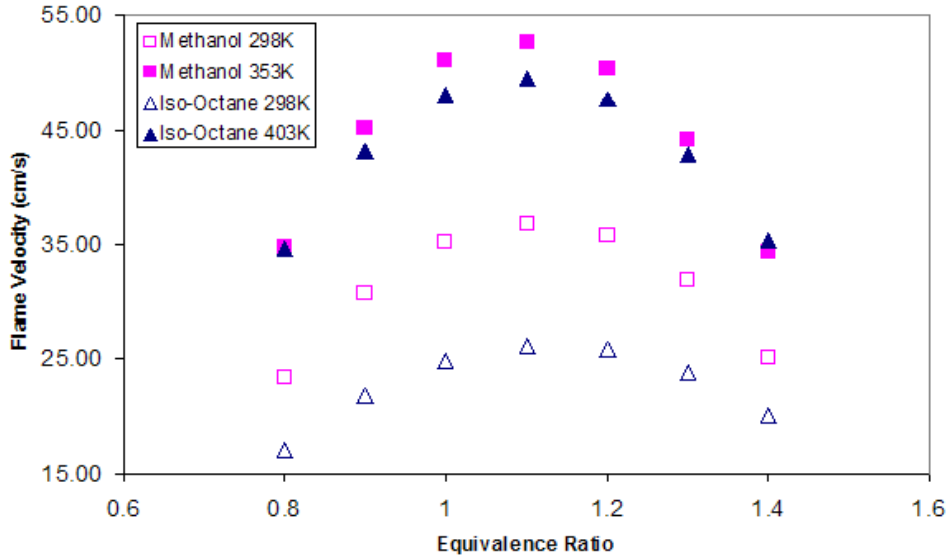

Figure 3.6: Flame speeds based on (Metghalchi and Keck, 1982).

moves slightly downstream with the increased flow rate, thereby reducing the distance to the thermocouple contributing to the higher temperature reading.

Alumina Beads

Replacing the alumina foam with 80mm of 3-3.5mm alumina beads on top of 20mm of 2-3mm diameter alumina beads resulted in the upper flammability limit being extended to 6.5. Once again the flame stabilized at the boundary between the two different ceramic layers. The operating envelope is illustrated in Fig.(3.8). As can be seen the flammability limit is extended further to the right and becomes wider than the foam operating envelope at the same ϕ. The maximum flame speed at ϕ=2.5 has now increased to 55cm/s compared to 40cm/s for the foam. As mention earlier, Drayton et al. (1998) used a uniform layer of ceramic beads with a moving flame front and

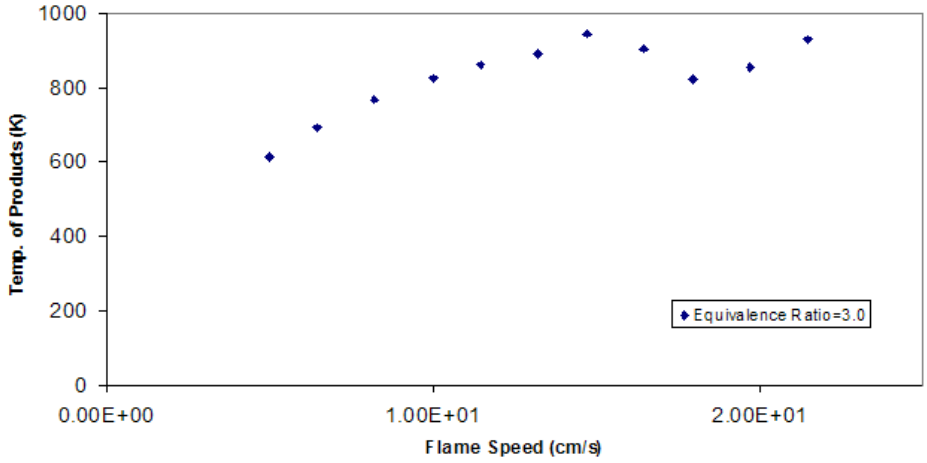

Figure 3.7: Temperature of the products versus flame speed at an equivalence ratio of 3.0.

methane.

This is surprising because theoretically the foams should be able to outperform the beads due to their higher thermal conductivity and lower optical thickness, resulting in overall superior heat transfer to the incoming gases. However, the beads used in this experiment cannot be considered solid spheres. These beads were manufactured to be used as a desiccant, which means that they have a large surface area ($300 m^2/gm$). Taking the mass of a measured volume of beads revealed that their actual porosity was 0.75, not 0.36 which is the approximate packing porosity for solid spheres. Therefore, 0.75 is used to calculate the flame speeds for the burner filled with beads. Possible explanations for the increased stability are: (1) higher convective heat transfer between the beads and incoming gas mixture due to the immense surface area and/or (2) additional reaction sites within the microporous surface for flames to stabilize on. At this point this is just con-

jecture, further tests with solid spheres need to be conducted to determine if it is the micropores on the surface of the beads that are enhancing the combustion process.

Based on a LHV of $21.6\times10^6 J/kg$ for CH_3OH, a firing range of $135kW/m^2$ to $2670kW/m^2$ was attained at an equivalence ratio of 2.5. This corresponds to a turndown ratio of 20:1. This high turndown ratio is possible because of the wide range of gas mixture speeds that the flame can stabilize at (eg. Fig.3.8). Trends suggest that even greater turndown ratios would be possible closer to stoichiometric conditions due to the broadening of the operating envelope.

At equivalence ratios above 4.5 no flame was visible inside the burner but the thermocouple above recorded a constant temperature. A plot of flame speed and temperature versus equivalence ratio is illustrated in Fig.(3.9). This plot was created by keeping the fuel flow rate constant and varying the air flow rates. As mentioned earlier this flame speed is not unique to each equivalence ratio. As can be seen the flame temperature drops with increasing ϕ and decreasing mass flow rate as there becomes less oxygen to react with the fuel and the flame moves slightly downstream.

In summary, it was possible to stabilize a flame at the interface between the two different pieces of ceramic. A wide operating envelope was observed that included flame velocities considerably higher than the laminar free flame velocity. This higher flame velocity is attributed to the increased heat transfer to the incoming reactants, which also contributes to the extension of the UFL. The alumina beads were able to support even faster flame velocities and higher UFLs. It is hypothesised that this increase in performance is related to the large surface area of the beads.

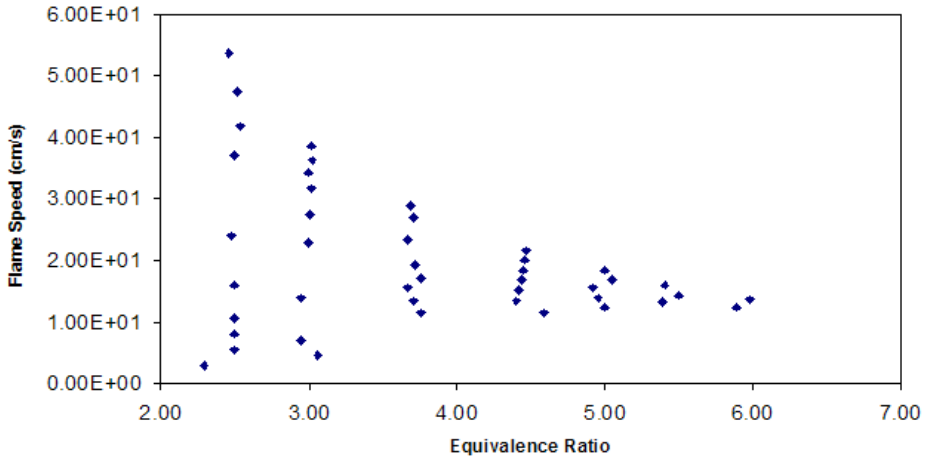

Figure 3.8: Operating envelope of methanol with 20mm of 2-3mm and 80mm of 3-3.5mm beads.

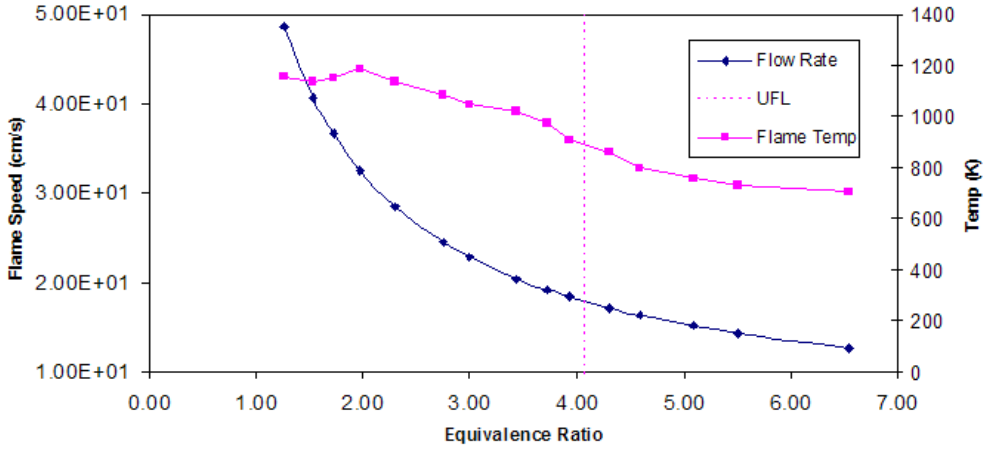

Figure 3.9: Methanol flame speed and temperature versus ϕ in the porous bead burner.

3.2.1 Octane and Petrol

Iso-Octane, 2,2,4-trimethyl pentane, is a hydrocarbon liquid that is used as a standard to measure the anti-knock qualities of petrol. Petrol is a mixture of hydrocarbons and other ingredients that manufacturers add to provide additional benefit. As a result the composition of petrol will vary from manufacturer to manufacturer and even from the same manufacturer, depending on the season and changes in regulations. Therefore, tests were conducted using iso-octane and also on the more complex mixture, petrol, since this is widely used in the transportation sector.

Alumina Foam

Octane and petrol both behaved similarly and stabilized at the interface between the two pieces of ceramic with the different PPI. Compared to a methanol flame which only takes a couple of minutes to enter the foam, the two hydrocarbon fuels took approximately 10 minutes to warm up the foam enough to propagate into it. Once stable, the upper flammability for the fuels could be attained as illustrated in Fig.(3.10) and Fig.(3.11). At equivalence ratios above 2.0 soot exiting the burner was visible, this is especially true of the petrol. The presence of soot inside the burner was also indicated by a bright yellow luminous flame, caused when the soot comes into contact with unburned oxygen and oxidizes. The soot accumulated on the thermocouple and turned the ceramics from white to black. However, the soot could be removed by burning a mixture with excess oxygen, lean mixture, for several minutes.

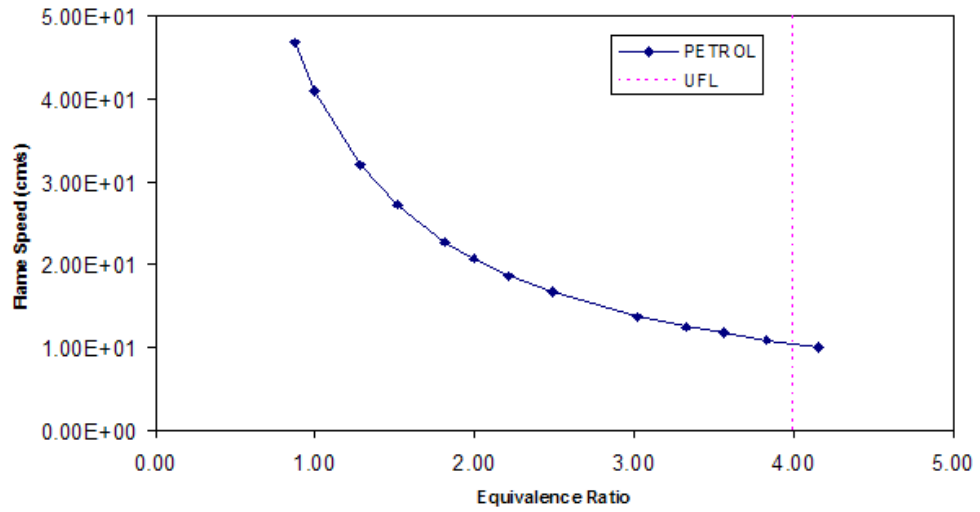

Figure 3.10: Petrol combusted inside a burner with 1x60PPI and 2x20PPI pieces of alumina. Note: density of iso-octane used to calculate flame speed.

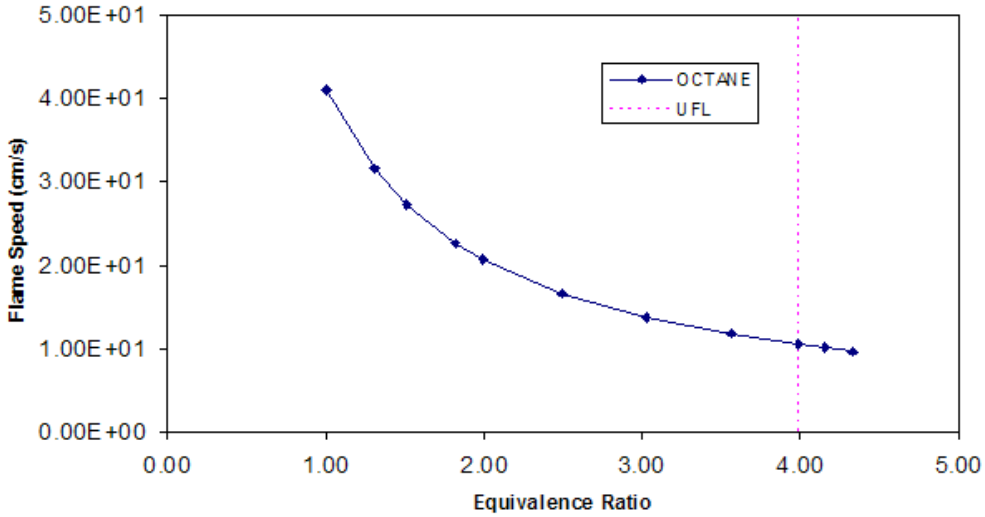

Figure 3.11: Iso-octane combusted inside a burner with 1x60PPI and 2x20PPI pieces of alumina.

Alumina Beads

It was not possible to get the flame to propagate into the ceramic using the 3-3.5mm alumina beads in the combustion region. Varying the flow rates at equivalence ratios close to stoichiometric conditions also proved unsuccessful. Placing a metal screen over the top of the burner to reduce thermal losses was also ineffective. Switching the beads back from the foams, resulted in the flame dropping into the ceramic again, verifying that it was the beads that were the culprit.

Iso-octane has a very large quenching diameter, approximately 4mm compared to 2mm for methanol (Glassman, 1987). Therefore switching to larger beads may allow the flame to propagate by increasing the spacing between the beads. However, larger beads also have a larger thermal mass requiring more energy to increase their temperature. Clearly a test using different sized beads needs to be conducted to prove which one is the dominant effect and to determine if the flame can propagate into the porous matrix.

In summary, the "proof of concept" has been achieved of combusting octane and petrol inside a porous media. Additional tests of foams with fewer PPI and larger diameter beads should reduce the quenching of the flames. The upper flammability limits attained compared to the literature values are tabulated in Table(3.1). '2-Alumina' refers to the two pieces of alumina used in the preliminary tests and '3-alumina' refers to the final configuration tested: one piece of small pore alumina and two pieces of large pore alumina.

	Free Flame*	2-Alumina	3-Alumina	Alumina Beads
	(UFL)	(UFL)	(UFL)	(UFL)
Methanol	4.08	3.5	4.4	6.5
Iso-Octane	3.8-4.2	-	4.0	-
Petrol	-	-	4.1	-

Table 3.1: Summary of experimental flammability limits compared to literature.
* Data obtained from references (Turns, 2000) and (API, 1976)

3.3 Materials Durability

The quartz burner proved to be very robust and showed no signs of degradation even after 100 plus hours of testing and over 200 complete thermal cycles (from ambient temperature to operating temperature). However, the stainless steel burner with the quartz window failed due to differing expansion and contraction rates of the materials.

The cordierite also failed but due to its melting temperature being exceeded. Alumina with its higher operating point did not melt or charr, but still suffered serious damage. After about 20 hours of testing it became more difficult to stabilize the flame at the ceramic interface. When attempting to remove the foam from the burner it started to crumble Fig.(3.12). This can be explained by two mechanisms: (1) because its thermal coefficient of expansion is approximately ten times higher that of quartz, stresses build up in the foam during expansion and contraction, and (2) sudden thermal gradients within the material due to ignition, cooling down periods, and changes in equivalence ratios can cause weakening or fracturing within the material. This is more pronounced in the alumina as it has a lower thermal shock resistance than cordierite.

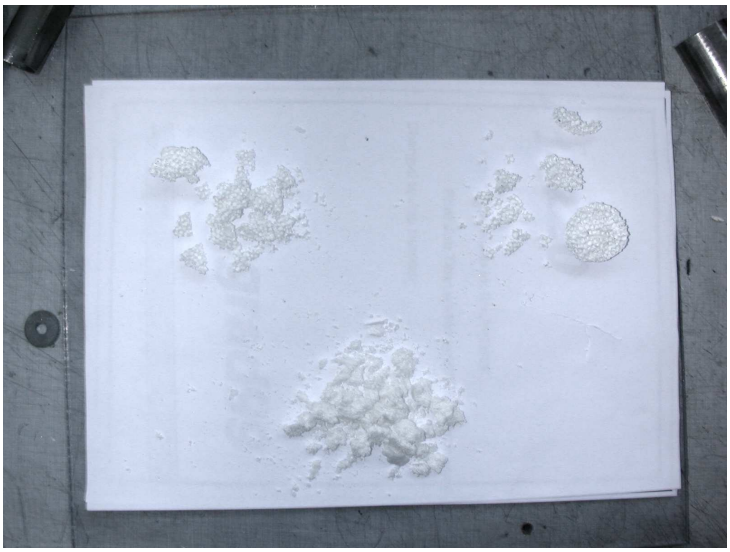

Figure 3.12: Damage to alumina.

The alumina beads appeared to suffer no degradation even after 100 plus hours of testing. Unlike the foams, which were held rigidly in place, the beads were free to move around inside the quartz burner. At higher flow rates the bed of beads would actually become fluidized and float on top of the incoming gas mixture. As a result the same stresses caused by thermal cycles did not build up inside the beads making them considerably more robust.

It can be concluded that generally beads will have a longer operational lifetime than foams as they are less susceptible to thermal stresses. However, the lifetime of the ceramic foams can be extended by selecting a burner material that has a similar thermal expansion rate.

3.4 Product Composition

Several tests were conducted in this phase of the project. The products of the three fuels were sampled by the gas chromatograph for a range of equivalence ratios within the operating envelopes. The results were compared to theoretical calculations using TPEQUIL, an equilibrium model based on (Olikara and Borman, 1975). These results were converted to a dry basis to compare to the results obtained from the GC. The probe height was also varied while maintaining the same flow rates for methanol and petrol to determine the effect on product concentrations. A GC printout of a methanol air mixture at ϕ=2.0 is included in Appendix C in Fig.(C.1) and Fig.(C.2). These two printouts correspond to the point at ϕ=2.0 in Fig.(3.13).

3.4.1 Methanol

Alumina Foam

Fig.(3.13) shows that up to an equivalence ratio of 3.0 the mole fraction of hydrogen and carbon monoxide increased with equivalence ratio while the mole fraction of carbon dioxide decreased. This reflects that the reaction is moving further away from completion due to lack of oxygen. After a ϕ of 3.0, H_2 started to decrease and CO_2 levelled off. Carbon monoxide also began to decrease after a ϕ of 3.5.

According to the equilibrium code hydrogen should continue to increase with ϕ even as the adiabatic flame temperature decreases. The adiabatic flame temperature was calculated using HPLAME, which is also based on Olikara and Borman (1975). The equilibrium code does not take hydrocarbons in the product into account, but in these tests insignificant amounts of hydrocarbons were detected. No hydrocarbons were measured in the prod-

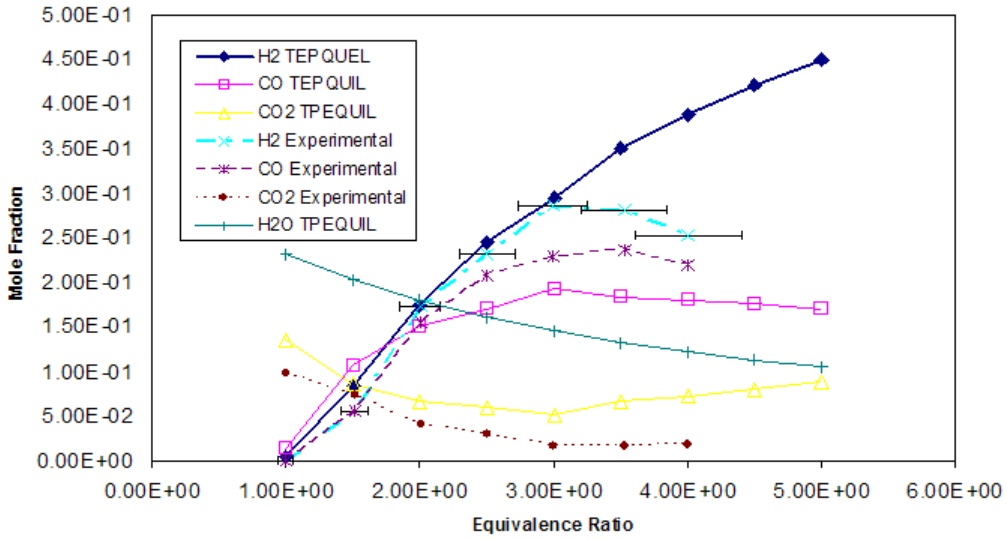

Figure 3.13: Comparison of TPEQUIL code at the adiabatic flame temp with experimental results (dry analysis) using methanol inside the alumina foam burner.

ucts at equivalence ratios less than 2.5. At a ϕ of 4.0 the largest concentration of hydrocarbons detected was methane at 0.6% with minute amounts of other hydrocarbons. Not enough to account for the low concentration of hydrogen measured. This may be an indication that the flame front is slowly moving upwards at these ultra-rich fuel conditions. These combustion products are plotted in Fig.(3.13). Error bars for ϕ were only placed on the experimental hydrogen measurements, but the same absolute values also apply to the other species detected by the GC. Flame speeds are the same as plotted in Fig.(3.9).

Changing the height of the sampling probe above the ceramic, at a ϕ of 2.5, did not result in any significant change in the product species or produce any discernable trends. This is a good indication that the products have reached equilibrium by the time they exit the ceramic and no more

reactions are taking place. However, it appears that at higher equivalence ratios the reaction has moved away from equilibrium. One way to verify this is to repeat the above the test at the higher ϕ.

Trace amounts of oxygen were also picked up by the GC for all tests, although thorough leak testing revealed no leaks in the system. The GC was not calibrated to detect oxygen but based on the area under the curve and the difference between the thermal conductivity of oxygen versus the reference gas, argon, the amount of oxygen in the samples is estimated to be much less than 0.1%. The GC is very sensitive to oxygen because its thermal conductivity is much greater than the reference gas's.

Alumina Beads

Fig.(3.14) shows that the product composition for these experiments followed the equilibrium calculations quite well and H_2 increased with increasing ϕ up to a ϕ of 5.0. At a ϕ of 6.0 the reaction moved away from equilibrium as it did at the higher equivalence ratios in the foam. The points at $\phi = 2.0$ and 2.5 need to be verified by repeating the tests, but the overall trend follows the equilibrium results. Flame speeds are the same as plotted in Fig.(3.9).

Although the experimental points are within the error bars, it appears as if it started to diverge from the code at equivalence ratios greater than 3.0. More CO, less CO_2 and less H_2 was generated than the equilibrium code predicted at the adiabatic flame temperature. According to equilibrium calculations as temperature increases, CO increases, while CO_2 and H_2 decrease as was seen here. Therefore, this is an indicating that the temperature in the burner was actually higher than the adiabatic temperature. Another indication that the reaction had reached a temperature greater than the adiabatic temperature is that the adiabatic temperature at $\phi = 5.0$ is 827K, but

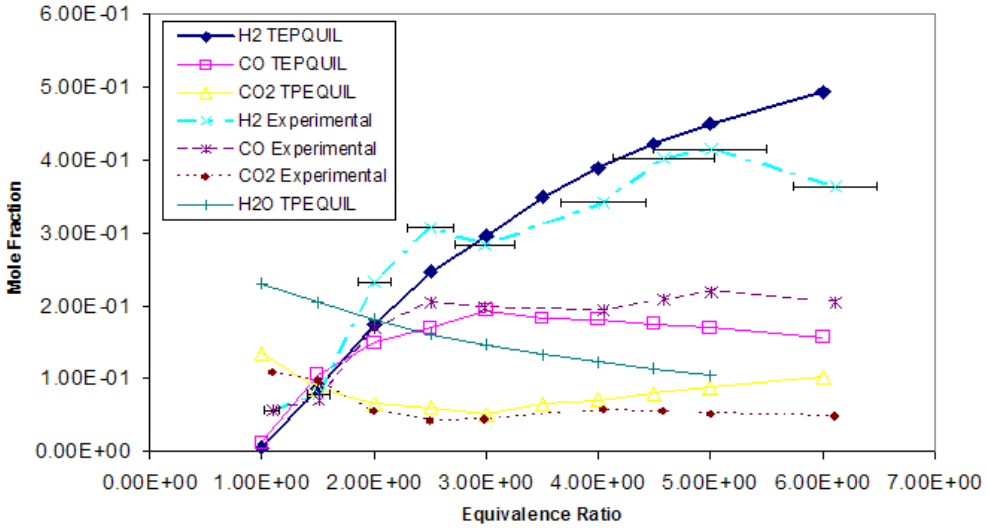

Figure 3.14: Comparison of TPEQUIL code at the adiabatic flame temp with experimental results (dry analysis) using methanol inside the alumina bead burner.

the thermocouple above the ceramics measured a temperature varying from 860K to 940K depending on the flow rates. This would tend to concur with observations made (Bingue et al., 2002) and (Drayton et al., 1998). Better methods to measure the temperature of the gases inside the burner will be able to verify this in the next stage of the project.

Similar amounts of hydrocarbons and trace amounts of oxygen as measured in the foam burner were also detected. At equivalence ratios above 5.0, no flame or glowing beads were visible inside the burner but the thermocouple measured a constant temperature.

The maximum amount of hydrogen produced was 42% by volume. The other major product apart from nitrogen was 22% CO which can be used in an additional steam reformation step and converted to CO_2 and H_2. Hydrogen production essentially increases with increasing ϕ. As ϕ increases the

amount of nitrogen is also decreasing which accounts for part of the higher molar fraction of hydrogen in the products. This means that the burner may be more efficient at converting methanol to hydrogen at a lower equivalence ratio. Defining the function of the burner as being able to convert fuels and alcohols to H_2 and assuming that the CO produced can also be converted to H_2 in a future water-gas shift reaction, then the efficiency of the burner is given by Eq.(3.1). Hagan et al. (2000) and Ahmed and Krumpelt (2001) use the LHV of H_2 produced divided by the LHV of fuel to calculate conversion efficiency, but this is after the water-gas shift reaction has taken place.

$$\eta = \frac{\dot{m}_{H2} LHV_{H2} + \dot{m}_{CO} LHV_{CO}}{\dot{m}_{fuel} LHV_{fuel}} \tag{3.1}$$

Since mass is conserved, the molar quantities of species detected by the GC must be converted to mass fractions. First the average molecular mass of the products can be determined by Eq.(3.2)

$$\overline{MW} = \sum_{i=1}^{n} x_i MW_i \tag{3.2}$$

Then the individual mass fractions for the components can be calculated by

$$Y_i = \frac{x_i MW_i}{\overline{MW}} \tag{3.3}$$

Since the GC's analysis is done on a dry basis the theoretical molar fraction of H_2O calculated by the equilibrium code is assumed to be the amount of H_2O removed from the sample prior to entering the GC. This is valid as long as the reactions reach equilibrium.

These results are plotted in Fig.(3.15). According to the equilibrium code, hydrogen production continues to increase with ϕ although the slope starts to level off. Hydrogen production will continue to increase until all of the H_2O has been converted to H_2. Results from the equilibrium code reveals

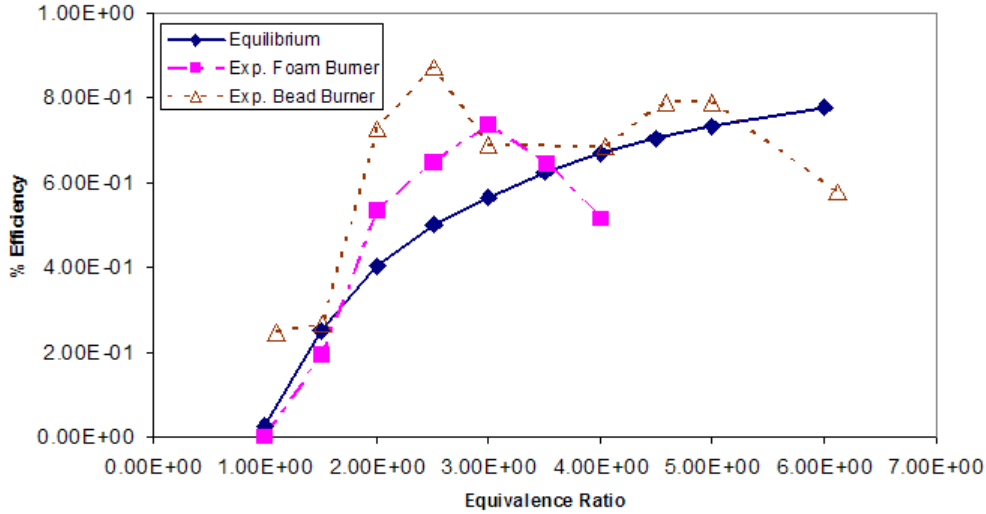

Figure 3.15: Efficiency of burners at producing hydrogen from methanol compared to equilibrium efficiency.

that this occurs at a very high ϕ for methanol. However, for a gas like CH_4 it occurs at ϕ=4.0 and for octane around a ϕ of 3.1.

In the foam burner at a ϕ=3.0, 74% of the lower heating value of the fuel is available in the H_2 and CO. The bead burner peaked at a ϕ=2.5 giving a conversion efficiency of 87%, however as mentioned earlier this point needs to be verified. Ignoring this point the maximum hydrogen conversion efficiency occurs at a ϕ of 5.0 converting 79% of the fuel to H_2 and CO. By optimizing the burner at higher ϕ, considerably more H_2 should be produced. The syngas stream at the burner's outlet will also be less diluted with N_2. Still the current efficiency of 79% for the bead burner is very impressive.

In summary, the reaction follows the equilibrium results at lower equivalence ratios but starts to deviate as the equivalence ratio is increased past 3.0 for the foam burner and 5.0 for the bead burner. High hydrogen con-

version efficiencies are possible for both burners. Superadiabatic combustion appears possible as product concentrations at higher ϕ correspond to flame temperatures higher than the adiabatic flame temperature. Additionally the thermocouple located above the ceramic recorded temperatures exceeding the adiabatic flame temperature.

3.4.2 Octane and Petrol

Alumina Foam

This time, with petrol, as the distance separating the probe and ceramics changed the product's composition also changed. Looking at Fig.(3.16), it can be seen that as the probe height increases the mole fraction of H_2, CO and minor hydrocarbon species all decrease, while the mole fraction of CO_2 increases. This is because the system has not reached equilibrium and chemical reactions for production and destruction of species are still occurring. As the distance increases, the reaction moves closer to completion as more species become oxidized. This has future implications as to where the ideal place to sample the gases are and if they should be cooled or not to optimize the H_2 production.

The product compositions of both the octane and petrol were very similar as is illustrated in Fig.(3.17) and Fig.(3.18) respectively. The plot for the petrol stops at a ϕ of 3.5 because this was one of the final tests run and the alumina foam was starting to degrade at this point reducing the flame's stability.

Hydrogen production peaked at 10% for petrol and slightly higher 11% for octane, much lower than the equilibrium code predicted. After an equivalence ratio of approximately 1.5 the actual hydrogen mole fraction started

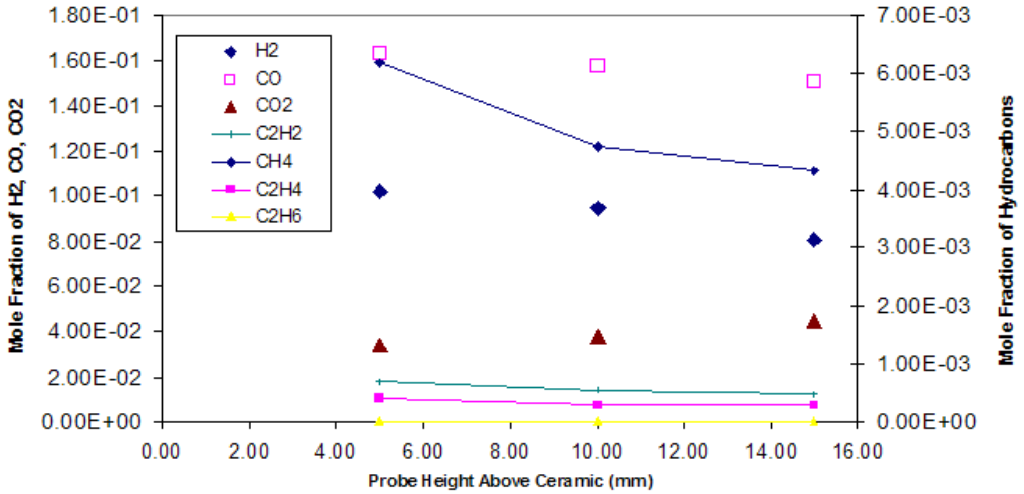

Figure 3.16: Combustion products of petrol in a porous foam burner versus probe height at an equivalence ratio of 1.5.

to diverge from the hydrogen predicted by the equilibrium code. However, the code does not take into account any other hydrocarbon species in the product. Soot was visible at ϕ above 2.0 for petrol and above 3.0 for octane. Fig.(3.19) and Fig.(3.20) shows that significant amounts of minor species are detected by the GC. Methane, acetylene and ethylene were the most abundant hydrocarbons detected, ethane peaked at 0.1%. Methane started to increase at a ϕ of 1.5 and continued to increase with ϕ. Ethylene started increasing at a ϕ of 2.5 and also continued to increase with ϕ. Acetylene increased rapidly from a ϕ of 1.5, peaked at a ϕ of 2.0 and then slowly decreased thereafter.

A carbon balance was performed using two different methods. In the first method, the carbon mass fraction of the reactants was calculated using

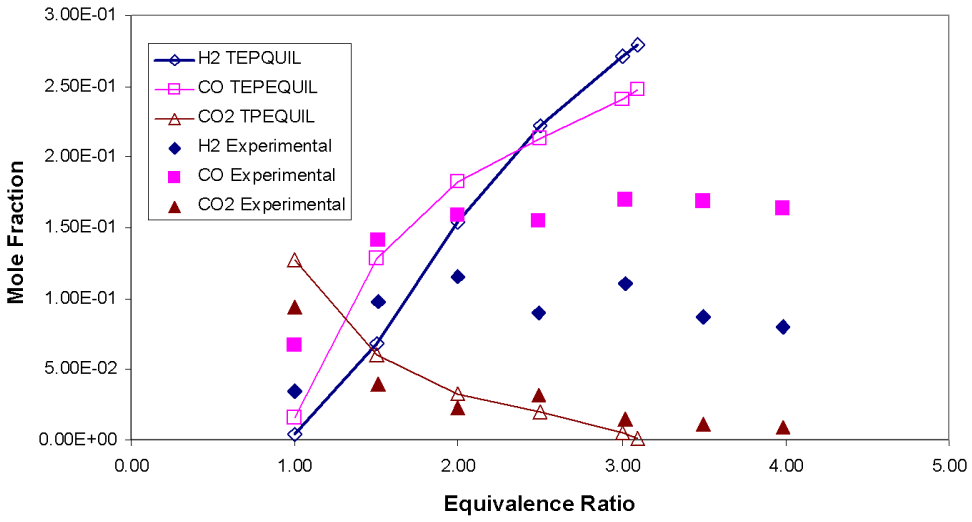

Figure 3.17: Comparisons of TPEQUIL code, C_8H_{18}, at the adiabatic flame temperature and experimental results (dry analysis) for octane in a porous foam burner.

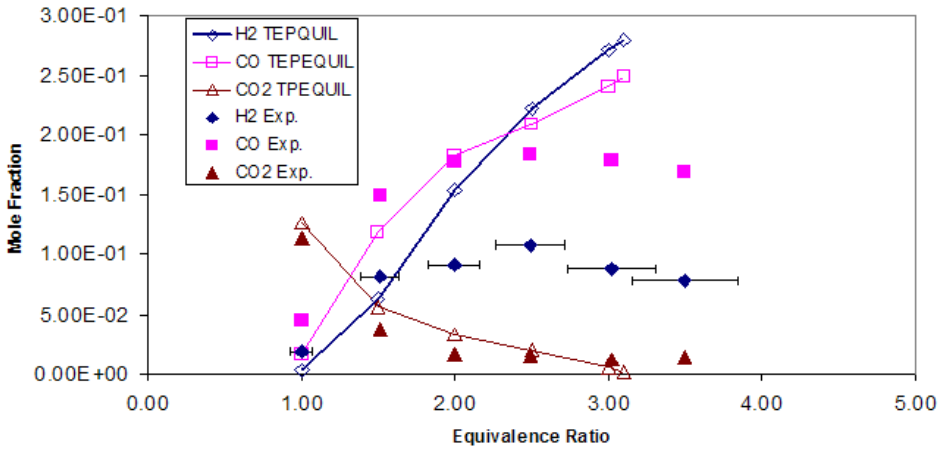

Figure 3.18: Comparisons of TPEQUIL code, C_8H_{18}, at the adiabatic flame temperature and experimental results (dry analysis) for petrol in a porous foam burner.

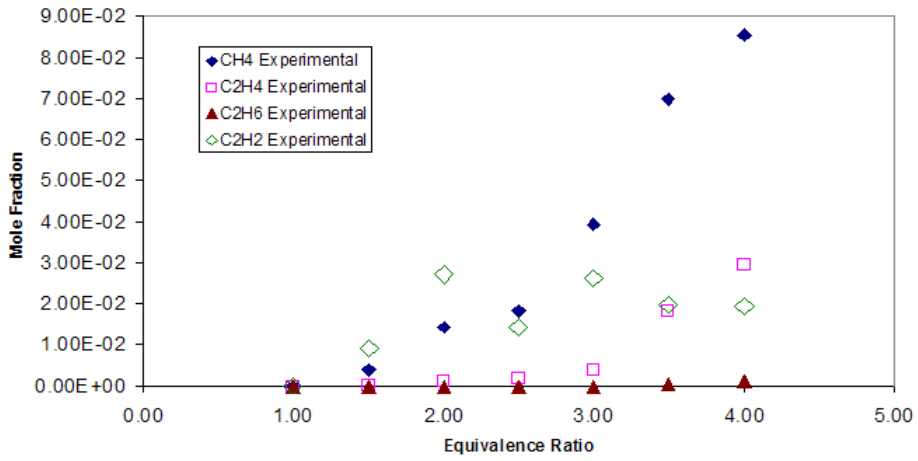

Figure 3.19: Minor species produced (Dry Analysis) by combustion of octane in a porous foam burner.

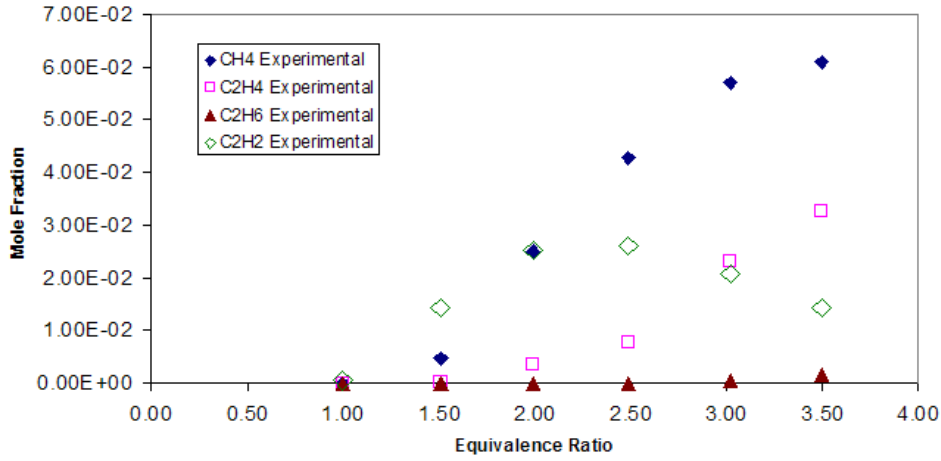

Figure 3.20: Minor species produced (Dry Analysis) by combustion of petrol in a porous foam burner.

$$Y_C = \frac{(\#\, of\, C)(MW_C)(Y_{C8H18})}{\overline{MW}_{C8H18}} \tag{3.4}$$

where the mass fraction of C_8H_{18} can be determined from

$$Y_{C8H18} = \frac{1}{1 + AFR/\phi} \tag{3.5}$$

Since mass and the number of elements are conserved, the mass fraction of carbon in the reactants should equal the mass fraction of carbon in the products. The molar fractions of CO, CO_2, CH_4, C_2H_2 and C_2H_6 measured by the GC were converted to a mass fraction by using the following equation

$$Y_C = \frac{X_{CO}MW_C + X_{CO2}MW_C + \sum X_{CxHy}MW_C}{\overline{MW}} \tag{3.6}$$

where $\bar{MW}$ is the average molecular weight of the products determined by multiplying the MW of the individual molecules in the product stream by their molar fractions and assuming anything not measured to be N_2 according to the following

$$\begin{aligned}\overline{MW} = X_{CO}MW_{CO} + X_{CO_2}MW_{CO2} + \sum X_{CxHy}MW_{CxHy} + \\ (1 - X_{CO} - X_{CO2} - \sum X_{CxHy})MW_{N2}\end{aligned} \tag{3.7}$$

However, since the H_2O has been removed from the sample prior to entering the GC, the mass fractions of the other species will be artificially high.

The second method calculates the amount of H_2O present in the products (since the reaction is not at equilibrium the amount of H_2O in the products is also different from what the code predicts) by performing an oxygen balance and using the measured molar fractions of the other products to solve for the molar fraction of water that was extracted prior to entering the GC. A more in depth analysis is performed in Appendix B.

The equilibrium model predicts H_2O will start at a mole fraction of 13.4% at a ϕ of 1.0 and decrease to zero by a ϕ of 3.1. However, based on the calculation for the experimental results, H_2O starts at a higher mole fraction, decreases to a mole fraction of approximately 13% by a ϕ of 2.0 and then remains steady. This results in a considerable amount of the H_2 being tied up in the H_2O and the other hydrocarbons that are not accounted for by the equilibrium code.

Once the amount of H_2O has been calculated a carbon and hydrogen balance can be performed using Eq.(B.17) and Eq.(B.18) in Appendix B. Fig.(3.21) is a plot of the molar amounts of carbon products from iso-octane normalized per mole of fuel using both the afore mentioned methods. As is expected the first method overestimates the amount of carbon present in the products especially at lower equivalence ratios where the amount of H_2O in the products is higher. Additionally, hydrocarbons not measured by the GC have higher molecular weights than the species measured, resulting in a further overestimation of carbon. It should be noted that even at stoichiometric conditions small amounts of hydrocarbons are present since the reaction does not reach equilibrium. The decrease in carbon at ϕ of 2.0 coincides with the appearance of soot.

The hydrogen production efficiency for octane was calculated based on Eq.(3.1) which accounts for the potential energy inside the H_2 and CO. However, since such a large amount of the hydrogen becomes tied up in other hydrocarbons the equation was modified to include the energy inside these species according to:

$$\eta = \frac{\dot{m}_{H2} LHV_{H2} + \dot{m}_{CO} LHV_{CO} + A}{\dot{m}_{fuel} LHV_{fuel}} \tag{3.8}$$

where

$$\mathrm{A} = \dot{m}_{CH4} LHV_{CH4} + \dot{m}_{C2H2} LHV_{C2H2} + \dot{m}_{C2H4} LHV_{C2H4} + \dot{m}_{C2H6} LHV_{C2H6}$$

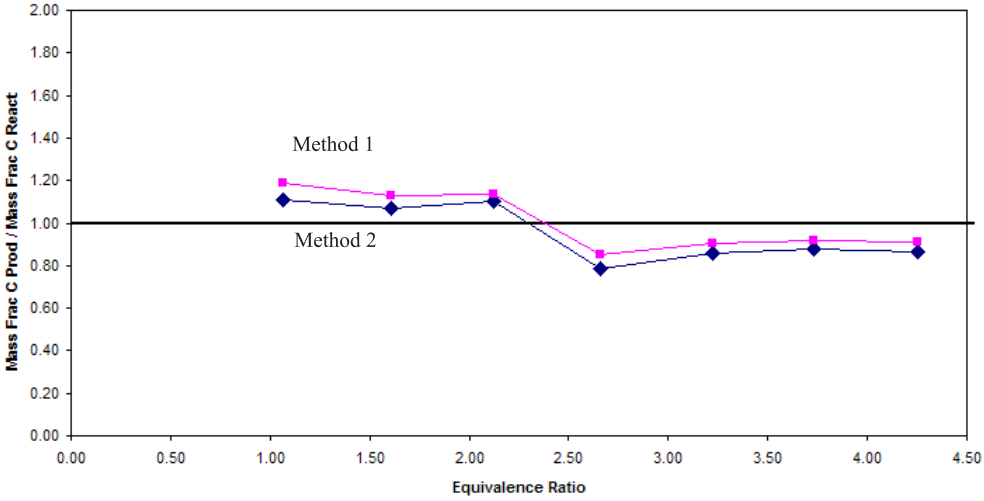

Figure 3.21: Normalized H and C products from Iso-Octane combusted in a porous foam burner.

This equation was used for comparative purposes to illustrate how much energy is stored in the additional hydrocarbons.

Fig.(3.22) illustrates that H_2 production efficiency peaks at 40% at a ϕ of 1.5, however when the additional hydrogen stored in the hydrocarbons is taken into account the potential hydrogen efficiency peaks at a much higher 75% at a ϕ=4.0. At a ϕ=4.0 the difference between the two curves is a maximum as this is also were the most hydrocarbons were produced. A second peak of 72% at a ϕ of 2.0 is also present. These double peaks resemble the ones observed in the methanol bead burner at a ϕ of 2.5 and a ϕ of 5.0, see Fig.(3.15).

Currently, because of the equipment's limitations it was not possible to keep the mass flow rate constant while varying the equivalence ratio. In future tests, it may be possible to optimize the hydrogen production by

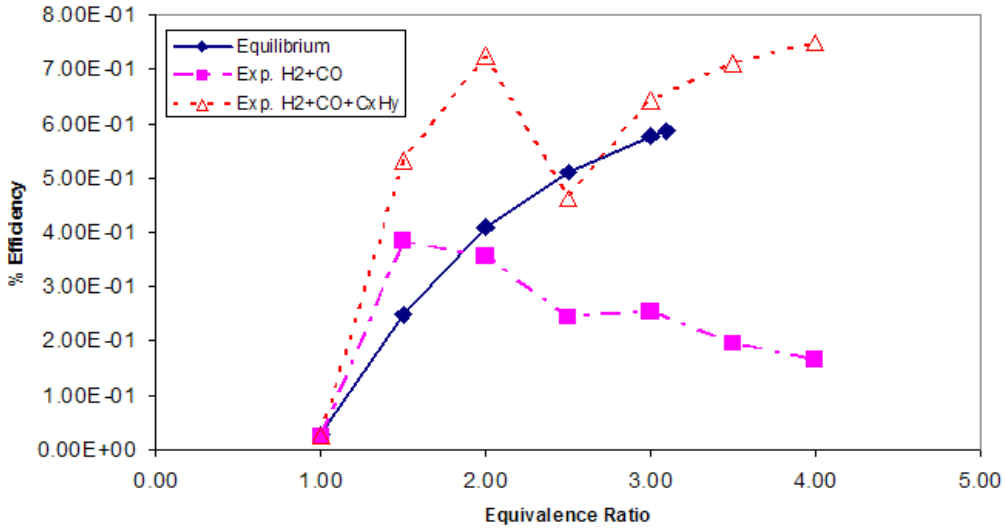

Figure 3.22: Efficiency of burner at producing hydrogen from octane compared to equilibrium efficiency.

varying the residence time of the gases and the burner geometry.

Octane's hydrogen production efficiency should be at a maximum when all the water has been converted to hydrogen and carbon monoxide. This should occur at a ϕ of approximately 3.1, according to the equilibrium model. But, in this case hydrogen efficiency continued to increase past a ϕ of 3.1 when accounting for the hydrogen stored in the other hydrocarbons.

The lower thermodynamic hydrogen production efficiency of the octane compared to the methanol is similar to results found by Epyx Corporation. They have demonstrated conversion efficiencies of 80% for petrol and 88% for methanol using an autothermal process (Hagan et al., 2000).

In summary, petrol and octane start to deviate from equilibrium at a lower ϕ than methanol did. Considerable amounts of H_2 is trapped in H_2O and the hydrocarbons. This H_2 needs to be recovered to make this a viable

technology for extracting H_2 from petrol.

Chan (2003) also performed some experiments using the same alumina foam burner, except with methane as the fuel. High heat transfer to the incoming gases resulted in increased burning velocities and an extension of the maximum equivalence ratio from 1.6, free flame UFL, to 1.9 . Varying the probe height did not result in significant changes in the product species, indicating that the gas composition was stable after it exited the ceramic. Since it was not possible to reach a ϕ of 4.0 for CH_4, the theoretical optimal point for H_2 production, it was not possible to determine if the hydrogen production efficiency would have peaked twice as it did for CH_3OH and C_8H_{18}. Overall, the technology was proven to work for methane as a viable non-catalytic hydrogen conversion burner.

3.5 Particulates

Octane (Alumina Foam)

Atmospheric particles have long been recognized to cause respiratory problems. Generally, the smaller the particle size the deeper it can penetrate into the lungs, and the larger the adverse health effects. More recently soot, particulates that form during imperfect combustion, have also been linked to global warming (Jacobson, 2001).

Due to the large amount of unburnt hydrocarbons and soot a SMPS, scanning mobility particle sizer, was used to measure the size and concentration of particles in the octane combustion products. Plots of the number concentration of particles versus size at various equivalence ratios are illustrated in Fig.(3.23) and Fig.(3.24).

At stoichiometric conditions the amount of particles detected is negligible,

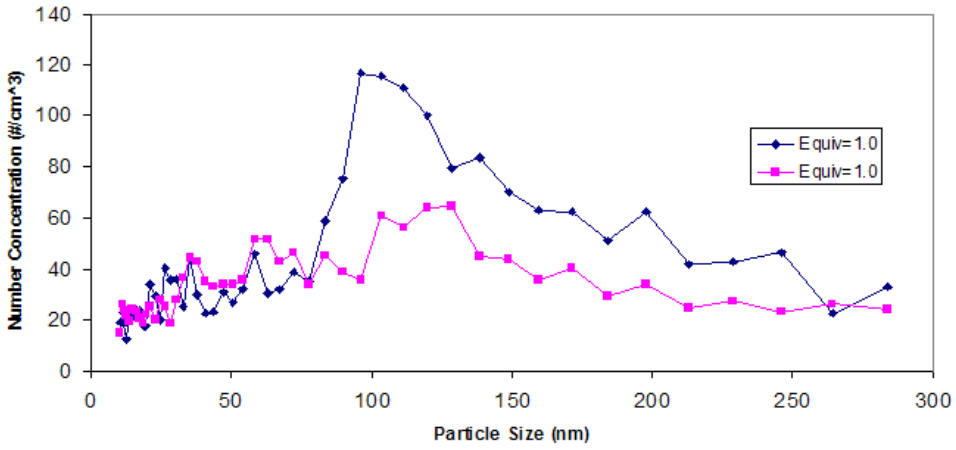

Figure 3.23: Particle number concentration versus size for octane at a ϕ of 1.0 in a foam burner.

as would be expected since all the carbon is being oxidized. The overall trend was for the particle number concentration and particle size to increase with ϕ as the reaction moved further away from completion. However, at a ϕ of 2.0 the particle concentration detected was approximately twice as high as at a ϕ of 2.5. Converting this to a mass per unit volume, revealed that more soot by mass was still being formed at a ϕ of 2.5. At an equivalence ratio of 2.0 the mass flow rate of reactants was about 70% higher than the mass flow rate at a ϕ of 2.5, making the resident time inside the combustion zone less. As a result the particles had less time to encounter other particles and join into larger species. Three separate tests at a ϕ of 2.0 and 2.5 were conducted to verify the repeatability of the instrument and experiment as a whole.

Therefore, varying the residence time of the gases inside the burner can be used to affect the particle size. For example, decreasing the flow rate would result in larger particles, for the same ϕ, that are less damaging to the

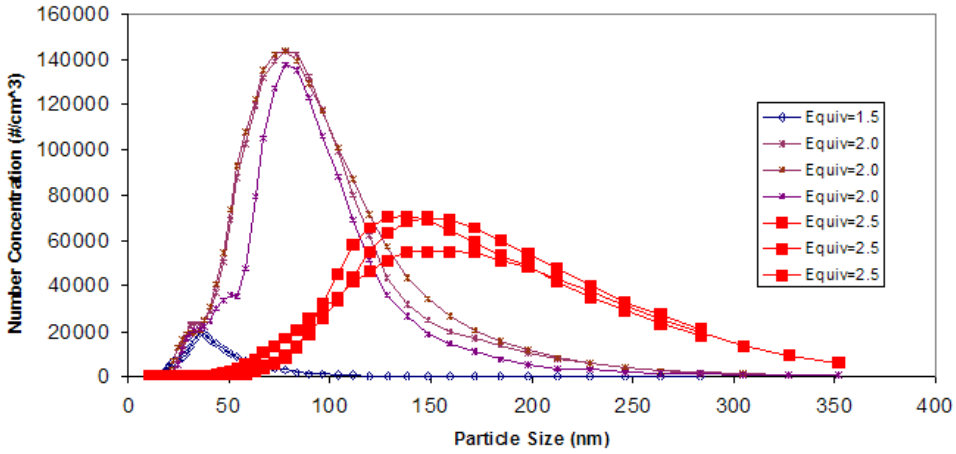

Figure 3.24: Particle number concentration versus size for octane at various ϕs in a foam burner.

respiratory system.

Chapter 4

Conclusions

It was possible to stabilize methanol flames inside both the alumina foams and beads at the interface between the two different sized pored ceramics and the different size beads. However, it was not possible to get the petrol and octane flames to propagate into the alumina beads. This is probably because of the large quenching diameter of these fuels. A large operating envelope encompassing much higher flame velocities than is possible with laminar free flames was observed. This resulted in a very high, 20:1, turndown ratio at an equivalence ratio of 2.5 for methanol.

It was determined that cordierite's melting temperature is too low to be used in a porous media burner. Alumina's melting point is adequate but alumina foams still undergo degradation due to stresses being built up because of thermal expansion and contractions. The alumina beads proved much more robust as they are not rigidly constrained and hence do not experience the same stress build up.

The upper flammability limit of methanol was dramatically increased by combustion in a porous media burner. At a minimum the conventional rich flammability limits for petrol and iso-octane were also reached.

Although theory predicted that the foams should be better at transferring heat to the incoming gases due to their higher conductivity because of bridging and lower optical thickness, it was actually the beads that produced the best results. At this point it is hypothesized that this extended UFL is due to the enhanced convective heat transfer between the beads and incoming gas mixture caused by the large surface area of the beads.

The maximum mole fraction of hydrogen was 24% from methanol and 11% from octane inside the porous foam burner. Using a conversion efficiency based on lower heating values, 74% of the methanol and 39% of the octane were converted to syngas. The maximum hydrogen yield was 42% for methanol inside the bead burner which is equivalent to a conversion efficiency of 79%. Both methanol and octane produced a second conversion efficiency peak at an equivalence ratio of approximately 2.0-2.5 indicating that residence time can also be used to optimize hydrogen conversion efficiencies. Optimizing the burner at the higher equivalence ratios should increase hydrogen production and reduce nitrogen dilution of the product stream.

Changing the height of the sample probe above the top ceramic had no effect on the methanol products indicating that the reaction was close to equilibrium at the exit of the ceramic. However, altering the height of the probe when octane was being combusted changed the products exiting the burner indicating that the reaction had not reached equilibrium and reactions were still occurring at the exit of the ceramics.

These results show that rich combustion inside a porous medium is a viable alternative to steam reforming and catalytic combustion for producing hydrogen. Quick startup times, compact size and high turn down ratios make it an ideal candidate for the next generation fuel cell powered automobile. The high conversion rates and wide variety of fuels that can be reformed also

gives it applications in the petroleum refinery industry.

Recommendations for Future Work

Thus far this project has proved that it is possible to extend the flammability limits of fuels by combustion inside porous media. It has also been possible to produce significant amounts of hydrogen from various fuels. However, the technique can be improved by enhancing and altering the existing apparatus as well as conducting additional testing and modelling.

Several improvements can be made to the burner. Placing an ignition source at the interface between the fine and course ceramics will improve safety and also should reduce the time it takes for the flame to stabilize. A larger diameter burner should improve the combustion process as less heat will be lost to the environment. Also by switching to a large diameter burner, higher flow rates will be possible that can be measured and controlled more accurately than the small flow rates used thus far.

Switching to an electronic mass flow controller will decrease the uncertainty associated with the air flow measurements which are currently the largest source of uncertainty. Similarly, switching to a more accurate and smoother pump will result in a more stable flame. These changes will allow the flow rates to be changed independently of the equivalence ratio. As mentioned in the method section, the current vaporizer may not always result in a steady continuous flow of vaporized fuel at lower flow rates. Converting to a more precise vaporizer should further increase the flame's stability.

Thermocouples placed inside a ceramic tube, to minimize the effects of radiation, should be located in the centre of the burner at 5mm intervals to get a better understanding of the flame's location and its temperature.

A chemiluminescence analyser to measure the NO_X emissions for several conditions would also be beneficial. All of these new measurement points should be continuously recorded by an automated data acquisition system, such as Labview.

As the other main products of rich combustion are CO and heat, it may be possible to vaporize H_2O with the waste heat and inject steam downstream of the combustion zone to convert the CO and H_2O into more H_2 and CO_2 via the water gas-shift reaction. Using the heat generated by the exothermic reaction to convert the water into steam will turn the system into an autothermal system with potential higher hydrogen production rates. The only disadvantages of this approach is that a catalyst will be required and the overall system will be slightly more complicated.

On the testing side, tests need to be conducted to determine why the beads are able to extend the upper flammability limit further than the foams. These tests should include testing with solid spherical alumina beads to determine if it is the large surface area of the beads that enhances the heat transfer and flame stability or another factor. A variety of bead sizes need to be tried to induce a petrol and octane flame to stabilize inside the ceramic.

Different flow rates at the same equivalence ratio need to be tested to try and optimize the hydrogen production and minimize the hydrocarbons present in the product especially from the octane and petrol products. The process also needs to be optimized to reduce soot production as soot can cause respiratory ailments and is also being linked to global warming.

Modelling with more advanced codes such as NASA's CEA code which can account for hydrocarbons in the products need to be investigated. A full kinetic model of the chemistry for rich combustion would also be most beneficial in helping to understand current experimental results and improving

the design of future burners.

These improvements to the apparatus, extended testing and modelling will increase the overall understanding of combustion inside porous media. This work will also help to bring the technology to the commercial market, where it should have a positive impact on hydrogen production for both the future hydrogen economy and also in today's refining operations.

Appendix A

Flame Speed Correlations

In free flames, flame temperature and laminar velocity are a function of the equivalence ratio and the initial pressure and temperature of the incoming reactants. In porous media they are also dependent on flow velocity and porous particle diameter. At steady state conditions, the laminar flame velocity is equal to the flow speed of the reactants in the free area space divided by the porosity of the porous media.

Metghalchi and Keck (Metghalchi and Keck, 1982) experimentally determined laminar flame speeds for several fuels at various fuel-air mixtures and temperatures. A modified version of their most useful correlation for calculating laminar flame speeds over a range of temperatures and equivalence ratios is given below

$$S_L = S_{L,ref} \left(\frac{T_u}{T_{u,ref}} \right)^{\gamma} \tag{A.1}$$

The subscript ref refers to standard temperature and pressure conditions.

$$S_{L,ref} = M_M + B_2(\phi - \phi_M)^2 \tag{A.2}$$

and

$$\gamma = 2.18 - 0.8(\phi - 1) \tag{A.3}$$

the constants B_M, B_2 and ϕ_M depend on fuel type and are given in Table (A.1).

Fuel	ϕ_M	B_M (cm/s)	B_2 (cm/s)
Methanol	1.11	36.92	-140.51
Isoctane	1.13	26.32	-84.72

Table A.1: Values for B_M, B_2 and ϕ_M used with Eq.(A.3).

(Metghalchi and Keck, 1982)

Appendix B

Non Equilibrium H_2O Calculation

The first step in performing a hydrogen and carbon balance on a non-equilibrium reaction, to determine if all the product species have been accounted for, is to calculate the amount of H_2O present in the products. The following equations assume: (1) No other species present in the products other than those listed in Eq.(B.1) and (2) N_2 does not participate in the reaction. The general equation for rich combustion with the additional hydrocarbons that the GC can measure can be written in the form:

$$C_8H_{18} + \frac{12.5}{\phi}(O_2 + 3.76N_2) \rightarrow a_1CO_2 + a_2CO + a_3H_2O + a_4H_2 + a_5O_2 + \frac{3.76 * 12.5N_2}{\phi} + a_6CH_4 + a_7C_2H_2 + a_8C_2H_4 + a_9C_2H_6 \quad \text{(B.1)}$$

Since the concentration of O_2 is minimal in the products it can be ignored. An oxygen balance on the equation can be written as

$$\frac{25}{\phi} = 2a_1 + a_2 + a_3 \quad \text{(B.2)}$$

Total number of moles is

$$n = a_1 + a_2 + a_3 + a_4 + \frac{47}{\phi} + a_6 + a_7 + a_8 + a_9 \tag{B.3}$$

The molar quantities are related to the measured dry molar fractions by

$$\begin{aligned} X_{CO2} = \frac{a_1}{n - a_3},\ X_{CO} = \frac{a_2}{n - a_3},\ X_{H2O} = \frac{a_3}{n} \\ X_{H2} = \frac{a_4}{n - a_3}, X_{CH4} = \frac{a_6}{n - a_3},\ X_{C2H2} = \frac{a_7}{n - a_3} \\ X_{C2H4} = \frac{a_8}{n - a_3},\ X_{C2H6} = \frac{a_9}{n - a_3} \end{aligned} \tag{B.4}$$

Using Eq.(B.2) and Eq.(B.3) gives

$$\frac{25}{\phi} - 2a_1 - a_2 = a_3 = n - a_1 - a_2 - a_4 - \frac{47}{\phi} - a_6 - a_7 - a_8 - a_9 \tag{B.5}$$

Solving for n results in

$$n = \frac{72}{\phi} - a_1 + + a_4 + a_6 + a_7 + a_8 + a_9 \tag{B.6}$$

Setting the molar quantities of Eq.(B.4) in terms of a_1 gives

$$\begin{aligned} a_4 = \frac{a_1 X_{H2}}{X_{CO2}}, a_6 = \frac{a_1 X_{CH4}}{X_{CO2}} \\ a_7 = \frac{a_1 X_{C2H2}}{X_{CO2}}, a_8 = \frac{a_1 X_{C2H4}}{X_{CO2}} \\ a_9 = \frac{a_1 X_{C2H6}}{X_{CO2}} \end{aligned} \tag{B.7}$$

Substituting these equations into Eq.(B.6) and rearranging gives

$$n = \frac{72}{\phi} - a_1 + \frac{a_1}{X_{CO2}} \left(X_{H_2} + X_{CH4} + X_{C2H2} + X_{C2H4} + X_{C2H6} \right) \tag{B.8}$$

Using

$$n = \frac{a_1}{X_{CO2}} + a_3 \tag{B.9}$$

from Eq.(B.4) and substituting into Eq.(B.8) gives

$$\frac{a_1}{X_{CO2}} + a_3 = \frac{72}{\phi} - a_1 + \frac{a_1}{X_{CO2}} \left(X_{H_2} + X_{CH4} + X_{C2H2} + X_{C2H4} + X_{C2H6}\right) \tag{B.10}$$

Rearranging the term for a_2 from Eq.(B.4) results in

$$a_2 = X_{CO}(n - a_3) \tag{B.11}$$

Eq.(B.2) can be rearranged to solve for a_3 by

$$a_3 = \frac{25}{\phi} - 2a_1 - a_2 \tag{B.12}$$

n can be eliminated from the equation by substituting Eq.(B.9) into Eq.(B.11) giving

$$a_2 = X_{CO}(\frac{a_1}{X_{CO2}}) \tag{B.13}$$

This equation can then be substituted into Eq.(B.12) giving

$$a_3 = \frac{25}{\phi} - 2a_1 - X_{CO}\left(\frac{a_1}{X_{CO2}}\right) \tag{B.14}$$

This equation can then be substituted into Eq.(B.10) and a_1 can be solved for

$$a_1 = \frac{\frac{47}{\phi}}{\left(\frac{1}{X_{CO2}} - 1 - \frac{X_{CO}}{X_{CO2}} - \frac{1}{X_{CO2}}(X_{H_2} + X_{CH4} + X_{C2H2} + X_{C2H4} + X_{C2H6})\right)} \tag{B.15}$$

The results from Eq.(B.15) can be substituted into Eq.(B.14) to solve for a_3. a_3 can then be used directly in Eq.(B.16) to determine the molar fraction of H_2O

$$X_{H2O} = \left(\frac{a_3}{n}\right) \tag{B.16}$$

The above calculations were checked with the equilibrium code and predict the same amount of H_2O as the code does. These equations were then used to calculate the amount of H_2O in the octane products based on the equivalence ratio and other products that the GC detected.

A carbon and hydrogen balance can now be performed based on Eq.(B.17) and Eq.(B.18) respectively.

$$\begin{aligned} No.\ of\ C = a_1(1) + a_2(1) + X_{CH4}(n) + \\ X_{C2H2}(2)(n) + X_{C2H4}(2)(n) + X_{C2H6}(2)(n) \end{aligned} \tag{B.17}$$

$$\begin{aligned} No.\ of\ H = a_3(2) + X_{H2}(2)(n) + X_{CH4}(4)(n) + \\ X_{C2H2}(2)(n) + X_{C2H4}(4)(n) + X_{C2H6}(6)(n) \end{aligned} \tag{B.18}$$

The math in these formulas were also verified by running the equilibrium code and confirming that the both the hydrogen and oxygen balanced.

Appendix C

GC Sample Printouts

Software Version	: 6.2.0.0.0:B27	Date	: 23/07/2003 12:14:49
Sample Name	:	Data Acquisition Time	: 13/05/2003 12:19:14
Instrument Name	: Autosystem	Channel	: A
Rack/Vial	: 0/0	Operator	: HAAKON
Sample Amount	: 1.000000	Dilution Factor	: 1.000000
Cycle	: 1		

Result File : C:\TCDATA\Test Data3\13May03_A001.rst
Sequence File : C:\TCDATA\Sequence\28mar.seq

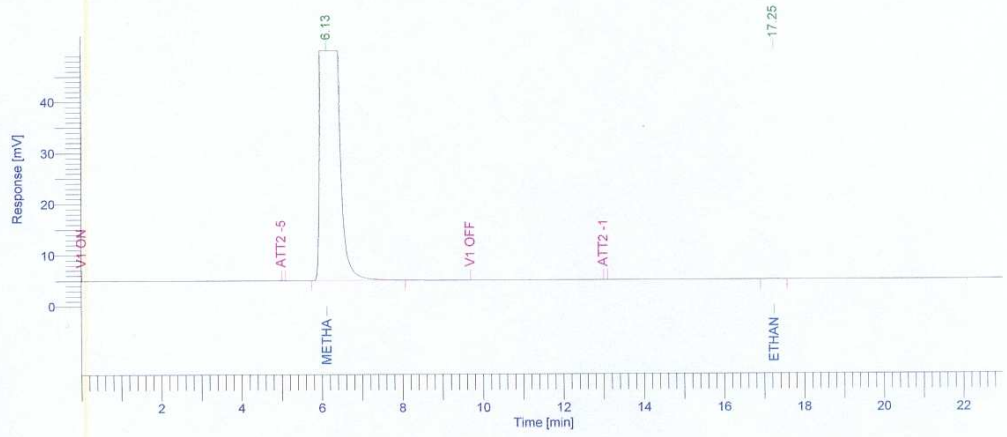

FID GAS ANALYSIS REPORT

Peak #	Component Name	Time [min]	Area [uV*sec]	% Concentration
1	METHANE	6.130	6409080.19	10.2521
-	ETHYLENE	14.655	0.00	0.0000
2	ETHANE	17.254	1121.63	0.0010
-	ACETYLENE	20.131	0.00	0.0000
			6410201.82	10.2530

Missing Component Report

Component	Expected Retention (Calibration File)
ETHYLENE	14.655
ACETYLENE	20.131

Figure C.1: GC FID printout of unlit 10% methane in air mixture.

Software Version	: 6.2.0.0.0:B27	Date	: 23/07/2003 12:16:00
Sample Name	:	Data Acquisition Time	: 13/05/2003 12:19:14
Instrument Name	: Autosystem	Channel	: B
Rack/Vial	: 0/0	Operator	: HAAKON
Sample Amount	: 1.000000	Dilution Factor	: 1.000000
Cycle	: 1		

Result File : C:\TCDATA\Test Data3\13May03_B001.rst
Sequence File : C:\TCDATA\Sequence\28mar.seq

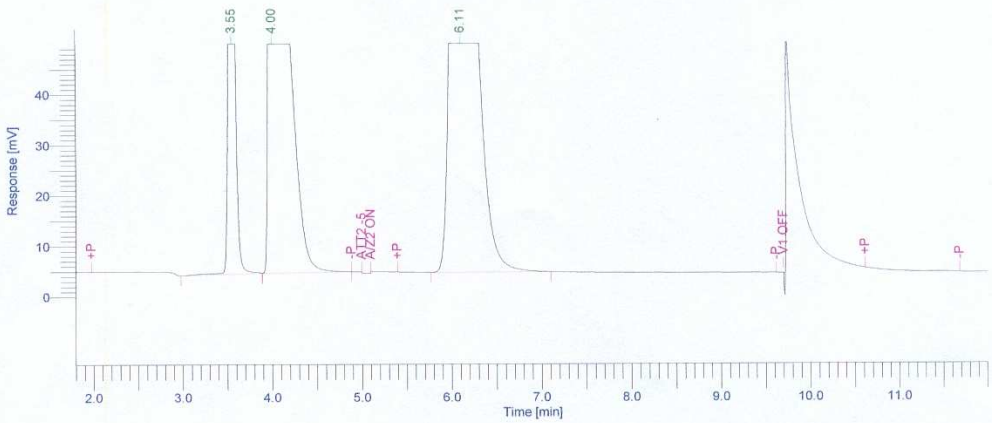

TCD GAS ANALYSIS REPORT

Peak #	Component Name	Time [min]	Area [uV*sec]	% Concentration
-	HYDROGEN	2.651	0.00	0.0000
-	CO	8.356	0.00	0.0000
-	CO2	11.236	0.00	0.0000
			0.00	0.0000

Missing Component Report

Component	Expected Retention (Calibration File)
HYDROGEN	2.651
CO	8.356
CO2	11.236

Figure C.2: GC TCD printout of unlit 10% methane in air mixture.

Software Version	: 6.2.0.0.0:B27	Date	: 23/07/2003 12:15:28
Sample Name	:	Data Acquisition Time	: 08/04/2003 13:05:14
Instrument Name	: Autosystem	Channel	: A
Rack/Vial	: 0/0	Operator	: HAAKON
Sample Amount	: 1.000000	Dilution Factor	: 1.000000
Cycle	: 1		

Result File : C:\TCDATA\Test Data3\08Apr_A005.rst
Sequence File : C:\TCDATA\Sequence\28mar.seq

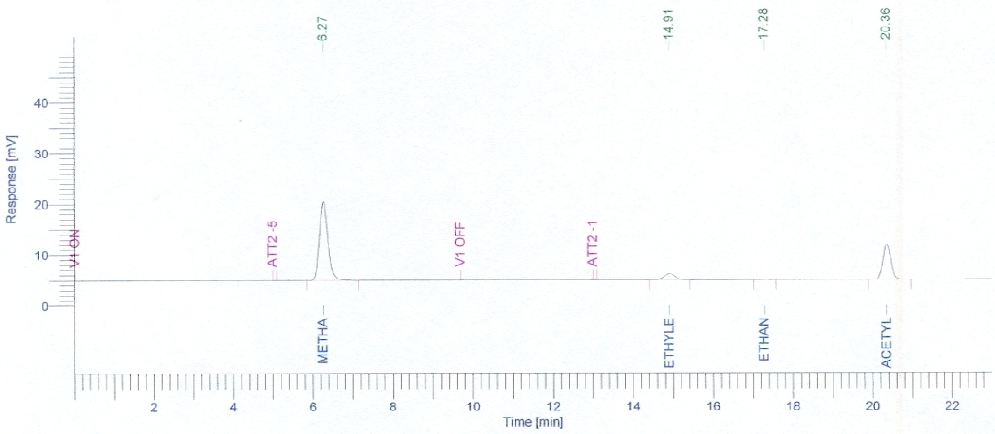

FID GAS ANALYSIS REPORT

Peak #	Component Name	Time [min]	Area [uV*sec]	% Concentration
1	METHANE	6.266	230489.10	0.3687
2	ETHYLENE	14.910	21383.03	0.0177
3	ETHANE	17.284	604.54	0.0005
4	ACETYLENE	20.356	94590.74	0.0788
			347067.42	0.4657

Missing Component Report

Component	Expected Retention (Calibration File)

All components were found

Figure C.3: GC FID printout of methanol at ϕ=2.0. Reference figure is Fig.(3.13).

Software Version	: 6.2.0.0.0:B27	Date	: 23/07/2003 12:13:32
Sample Name	:	Data Acquisition Time	: 08/04/2003 13:05:14
Instrument Name	: Autosystem	Channel	: B
Rack/Vial	: 0/0	Operator	: HAAKON
Sample Amount	: 1.000000	Dilution Factor	: 1.000000
Cycle	: 1		

Result File : C:\TCDATA\Test Data3\08Apr_B005.rst
Sequence File : C:\TCDATA\Sequence\28mar.seq

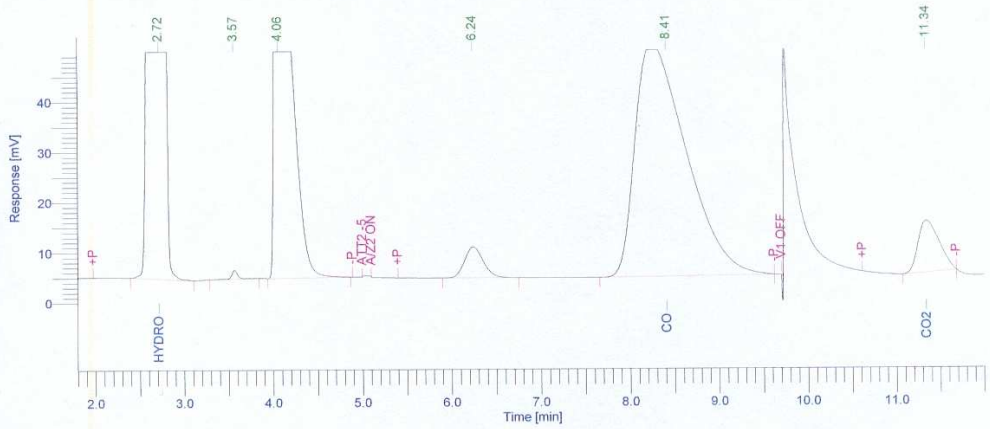

TCD GAS ANALYSIS REPORT

Peak #	Component Name	Time [min]	Area [uV*sec]	% Concentration
1	HYDROGEN	2.720	5371990.62	23.1676
5	CO	8.412	1842957.38	20.7520
6	CO2	11.341	170628.28	3.0235
			7385576.28	46.9431

Missing Component Report
Component Expected Retention (Calibration File)

All components were found

Figure C.4: GC TCD printout of methanol at ϕ=2.0. Reference figure is Fig.(3.13).

Bibliography

S. Ahmed and M. Krumpelt. Hydrogen from hydrocarbon fuels for fuel cells. *International Journal of Hydrogen Energy*, 26:291–301, 2001.

Anonymous. Flame temperature measurement experiment. Technical report, California Institute of Technology, 1994.

Anonymous. Gas chromatography. Technical report, Sheffield Hallam University, http://www.shu.ac.uk/schools/sci/chem/tutorials/chrom/gaschrm.htm, 2002.

API. Alcohols: A technical assessment of their application as motor fuels. Technical Report No. 4261, American Petroleum Institute, 1976.

V. S. Babkin, A. A. Korzhavin, and V. A. Bunev. Propagation of premixed gaseous explosion flames in porous media. *Combustion and Flame*, 87: 182–190, 1991.

A. Bansal, J. Beach, R. Collins, O. Khaselev, and J. A. Turner. Photoelectrochemical based direct conversion systems for hydrogen production. U.S. DOE Hydrogen Program Review, 1999.

M. Becker. *Heat Transfer a Modern Approach.* Plenum Press, 1st edition, 1986.

P. J. Berlowitz and C. P. Darnell. Fuel choices for fuel cell powered vehicles. In *Fuel Cell Technology for Vehicles*, volume PT-84 of *SAE International Progress in Technology Series*, pages 45–55, 2000.

J. P. Bingue, A. V. Saveliev, A. A. Fridman, and L. A. Kennedy. Hydrogen production in ultra-rich filtration combustion of methane and hydrogen sulfide. *International Journal of Hydrogen Energy*, 27:643–649, 2002.

G. Biskos. Calibration modification of the fast aerosol spectrometer. Technical report, Eng. Dept. University of Cambridge, 2001.

L. Chan. Hydrogen production by rich flame combustion for fuel cells. Technical report, Eng. Dept. University of Cambridge, 2003.

M. Cropper. Chrysler develops fuel cell van using novel hydrogen storage technology. *Fuel Cell Today*, Dec. 2001.

D. J. Diamantis, E. Mastorakos, and D.A. Goussis. Simulations of premixed combustion in porous media. *Combustion Theory and Modelling*, 6:383–411, 2002.

Doceram. http://www.doceram.com/e/ mat1.htm. Internet, 2003.

DOE. Hydrogen program overview. Technical Report DOE/GO-10095-088, Department of Energy, 1995.

M. K. Drayton, A. V. Saveliev, L. A. Kennedy, A. A. Fridman, and Y. Li. Syngas production using superadiabatic combustion of ultra-rich methane-air mixtures. *Twenty-Seventh Symposium on Combustion*, pages 1361–1367, 1998.

Dupont. Private phone conversation with dupont, 2002.

I. Glassman. *Combustion*. Academic Press, 2nd edition, 1987.

Goodfellow. http://www.goodgellow.com/csp/active/gfmaterialinfo.csp. Internet, 2003.

M. Hagan, W. Northrop, B. Bowers, J. Rumsey, and S. Prabhu. Automotive fuel processing for pem fuel cells. In *Fuel Cell Technology for Vehicles*, volume PT-84 of *SAE International Progress in Technology Series*, pages 103–110, 2000.

IEA. Moving to a hydrogen economy: Dreams and realities. Technical Report IEA/SLT 5, International Energy Agency, 2003.

Y. Itaya, T. Oyashiki, and M. Hasatani. Hydrogen production by methane-rich combustion in a ceramic burner. *Journal of Chemical Engineering of Japan*, 35(1):46–56, 2002.

M. Z. Jacobson. Strong radiative heating due to the mixing state of black carbon in atmospheric aerosols. *NATURE*, 409(6821):695–697, 2001.

S. J. Kline and F. A. McClintock. *Experimental Methods for Engineers*, volume 75, pp.3. McGraw Hill, New York, 1953.

P. Maness and P. F. Weaver. Biological hydrogen from fuel gases and from water. U.S. DOE Hydrogen Program Review, 1999.

M. Marquevich, S. Czernik, E. Chornet, and D. Montan. Hydrogen from biomass: Steam reforming of model compounds of fast-pyrolysis oil. *Energy & Fuels*, 13:1160–1166, 1999.

W. M. Mathis Jr. and J. L. Ellzey. Flame stabilization, operating range, and emissions for a methane/air porous burner. *Combustion Science and Technology*, 175:825–839, 2003.

M. Metghalchi and J.C. Keck. Burning velocities of mixtures of air with methanol isoctane and indolene at high pressures and temperatures. *Combustion and Flame*, 48:191–210, 1982.

R. A. Meyers. *Handbook of Petroleum Refining Processes*. McGraw-Hill, Toronto, 2nd edition, 1997.

Inc. Mindrum Precision. *Ceramic Properties*, 2003. http://www.mindrum.com/tech.html.

N. Z. Muradov. Carbon dioxide-free production of hydrogen by catalytic pyrolysis of hydrocarbon fuel. *Energy and Fuels*, 12:41–48, 1998.

C. Olikara and G.L. Borman. A computer program for calculating properties of equilibrium combustion products with some applications to i.c. engines. *SAE Paper*, 750468, 1975.

J. Piskorz, D. Scott, and D. Radlein. Pyrolysis oils from biomass: Producing, analyzing and upgrading. *ACS Symposium Series 376; American Chemical Society*, pages 167–178, 1988.

J. Rifkin. *The Hydrogen Economy*. Putnam Publishing Group, New York, 2002.

Sembach. http://www.sembach.de/uk/werkstoffe/cordierit/index.htm. Internet, 2003.

S. Springmann. http://www.icvt.uni−stuttgart.de/research/fuelcell/reforming.html. Stuttgart Institute for Chemical Processing Engineering, Dec. 2002.

A. Steinfeld. From solar to chemical energy. *Fuel Cell World Proceedings*, pages 356–366, 2002.

D. Trimis and F. Durst. Combustion in a porous medium-advances and applications. *Combustion Science and Technology*, 121:153–168, 1996.

D. Trimis, F. Durst, O. Pickencker, and K. Pickencker. Porous medium combustor versus combustion systems with free flames. ISHTEEC '97, 1997.

S. R. Turns. *An Introduction to Combustion*. McGraw-Hill, New York, 2nd edition, 2000.

N. B. Vargaftik. *Tables on the Thermophysical Properties of Liquids and Gases*. Nauka Press, Moscow, 2nd edition, 1975.

J. Vernes. *L'le Mystrieuse*. 3 vol. London, 1875.

J. P. Wagner and H. Takeda. Co purification for fuel cells using selective methanation catalysts. American Institute of Chemical Engineers Conference, 2001.

E. Weisstein. Sphere packing. http://mathworld.wolfram.com/spherepacking.html, 1999.

K. Zepter and J. E. Hustad. Combustion and emission studies in a porous inert media burner. *Meeting of the Scandinavian-Nordic Section of the Combustion Institute*, 2001.